





## Influence of direct dipole-dipole interactions on the optical response of two-dimensional materials in strongly inhomogeneous infrared cavity fields

Sofia Ribeiro <sup>1</sup>, Javier Aizpurua <sup>1,2</sup>, and Ruben Esteban <sup>1,2,\*</sup>

<sup>1</sup>Material Physics Center, CSIC-UPV/EHU, Paseo Manuel de Lardizabal 5, 20018 San Sebastián-Donostia, Basque Country, Spain

<sup>2</sup>Donostia International Physics Center, Paseo Manuel de Lardizabal 4, 20018 San Sebastián-Donostia, Basque Country, Spain

 (Received 19 April 2023; revised 10 July 2023; accepted 6 September 2023; published 20 October 2023)

A two-dimensional (2D) material, formed, for example, by a self-assembled molecular monolayer or by a single layer of a van der Waals material, can couple efficiently with photonic nanocavities, potentially reaching the strong-coupling regime. The coupling can be modeled using classical harmonic-oscillator models or cavity quantum electrodynamics Hamiltonians that often neglect the direct dipole-dipole interactions within the monolayer. Here we diagonalize the full Hamiltonian of the system, including these direct dipole-dipole interactions. The main effect on the optical properties of a typical 2D system is simply to renormalize the effective energy of the bright collective excitation of the monolayer that couples with the nanophotonic mode. On the other hand, we show that for situations of extreme field confinement, large transition dipole moments, and low losses, fully including the direct dipole-dipole interactions is critical to correctly capture the optical response, with many collective states participating in it. To quantify this result, we propose a simple equation that indicates the condition for which the direct interactions strongly modify the optical response.

DOI: [10.1103/PhysRevA.108.043718](https://doi.org/10.1103/PhysRevA.108.043718)

### I. INTRODUCTION

Light and matter couple strongly when a large number of molecules, a van der Waals material or a similar system, is placed within nanophotonic cavities [1,2]. In the strong-coupling regime, the wave functions of the photonic modes and the material excitations mix to form new hybridized collective states known as polaritons [2–6]. For example, the strong coupling between photonic modes and electronic molecular transitions results in the formation of excitonic polaritons [7–9]. Moreover, there is growing interest in vibrational polaritons that are due to the coupling of vibrational modes of molecules and infrared (IR) microcavities [10–13]. The emergence of these new IR polaritonic states can significantly impact the physical and chemical properties of the system [11,14–19], allowing for active manipulation of matter.

The optical properties of two-dimensional (2D) systems located in a cavity can be studied using cavity quantum electrodynamics (CQED) or via classical harmonic-oscillator models [20,21], which often neglect the direct dipole-dipole coupling between the different polarizing units, such as the molecules or the different regions of the material (unit cells). Within this framework, the system typically shows two optically bright polariton modes under strong enough coupling strength, whether we have one or an ensemble of polarizable units forming a 2D material. The energy of these polaritonic modes is different from those of the uncoupled nanocavity and the vibrational or electronic excitation in the material, and their energy difference (Rabi splitting) increases with the number  $N$  of polarizable units, approximately as  $\sqrt{N}$  in simple situations [22,23]. Additionally,  $N - 1$  dark modes

are also present that interact much more weakly with cavity photons, or not at all [24].

On the other hand, the direct dipole-dipole interactions between the polarizing units of the 2D material can also influence the optical response. In a simple example, applying the Clausius-Mossotti equation to an ensemble of molecules (or oscillators) indicates that the resonances of the classical permittivity are shifted from the energy of the individual oscillators [25]. This effect is considered implicitly, for example, in a recent work studying the coupling between collective lattice vibrations (phonons) in hexagonal boron nitride (h-BN) and microcavity modes [26]; the h-BN layer was treated as an ensemble of dipoles, with resonant energy defined by the classical permittivity, which served to take into account the dipole-dipole interactions in an effective manner. In a similar context, it was shown in Refs. [27,28] that a dense atomic cloud could be described as a homogeneous particle with an effective permittivity. In these works the authors showed that there is a correspondence between the microscopic polaritonic modes of the atomic cloud (obtained by considering dipole-dipole interactions between the atoms) and the modes of a homogeneous particle.

In this paper we use a microscopic CQED description of the dynamics of excited states to gain further insight into the effect of the direct dipole-dipole interaction on the optical response. We focus on the coupling of a nanophotonic cavity mode with vibrations of a 2D material (see Fig. 1), which could consist of a self-assembled molecular monolayer or a single layer of a van der Waals material. Van der Waals materials manifest very clear phonon modes with large reststrahlen bands that enable new optical properties [29–32], while molecular monolayers have applications in the design of different devices such as chemical sensors, biosensors, and organic field-effect transistors (see Ref. [33] and refer-

\*Corresponding author: [ruben.esteban@ehu.eus](mailto:ruben.esteban@ehu.eus)

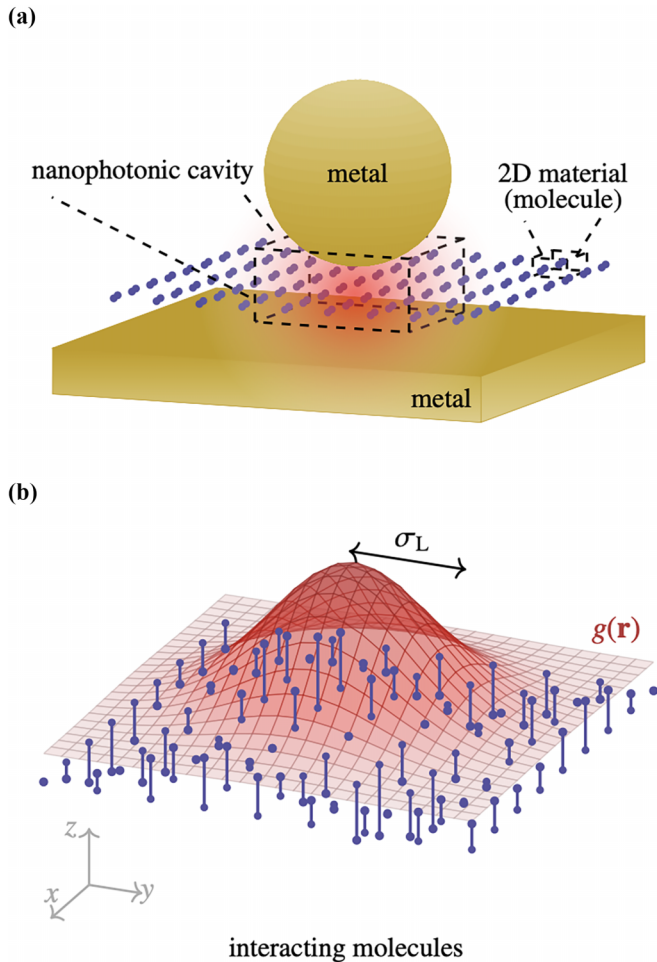


FIG. 1. System under study. (a) Schematic of an ensemble of  $N$  molecules placed in a 2D square lattice configuration inside a photonic (plasmonic or phononic) nanocavity. The cavity fields are represented by the red-shaded area. (b) Schematic of the excitation of the molecules by the nanocavity and the collective mode emerging from the direct dipole-dipole coupling between the molecules. The inhomogeneous cavity IR field varies as a function of position  $\mathbf{r}$  following a Gaussian distribution  $g(\mathbf{r})$  of width (standard deviation)  $\sigma_L$ , as represented by the red-colored surface. If the molecules interact with each other, a collective or cooperative vibronic behavior of the 2D molecular vibrations can emerge. Each resulting collective mode can then be seen as a density wave along the 2D plane forming a standing-wave pattern. The vertical lines illustrate the induced molecular dipoles corresponding to one such density wave. The schematics are not to scale.

ences therein). For simplicity, we often refer below directly to molecular assemblies, even if some values used for the parameters can be more representative of van der Waals materials. The cavity fields can present extreme spatial confinement, down to subnanometer regions, as occurs in plasmonic cavities formed by atomic-size protrusions (picocavities) in, e.g., scanning tunneling microscopy, nanoparticle-on-mirror constructs, or similar configurations [34–37]. We emphasize that our methodology is very general and the conclusions can be applied directly to other related situations, including the coupling with excitonic molecular transitions.

In the following we first describe in Sec. II a general theory of the coupling between vibrations in the 2D material and a nanocavity mode. The model treats the vibrations as pointlike dipoles, with each dipole corresponding to a molecule (or to a microscopic region of the 2D material, such as a unit cell [26,38]). The vibrations occur in the direction perpendicular to the 2D monolayer. In Sec. III we diagonalize the vibronic Hamiltonian in the absence of a nanophotonic cavity to obtain the new eigenmodes of the system, corresponding to the collective vibrational modes. We then include the cavity mode in Sec. IV and write the full interaction Hamiltonian as a function of these collective vibrational modes, which we solve to find the new vibron-polariton modes. Based on the properties of these modes, we obtain and analyze the optical response of the coupled system to reveal the effect of the direct dipole-dipole interaction. We summarize in Sec. V.

## II. THEORETICAL MODEL

We consider a patch of  $N$  molecules (polarizing units in the 2D material) that form a monolayer inside an IR nanophotonic cavity (e.g., a plasmonic or phononic nanoresonator), as sketched in Fig. 1(a). For our numerical simulations, we arrange  $N = 51 \times 51 = 2601$  molecules in a lattice of square unit cell with lattice constant  $a$  (which we fix at  $a = 0.5$  nm), placed in the  $xy$  plane. Each molecule is modeled as a dipole associated with a molecular vibration that is optically active at IR frequencies. The same model is also suited to treat other excitations, such as electronic transitions. The dipoles are oriented perpendicular to the  $xy$  plane, in the  $z$  direction. We consider perfectly regular arrays with dipoles oriented along a fixed direction, but we expect that small randomness in the position or orientation of the molecules would affect the results weakly.

If the molecules are sufficiently far apart from each other, the molecular vibrations (or the excitonic transitions) are typically assumed to interact much more efficiently with the localized cavity field than directly with each other. This localized field can be confined to a very small region [35], as represented schematically by the red-colored surface in Fig. 1(b), strongly increasing the coupling between the cavity and the molecules [34,36,39]. However, when the molecules are closely packed, the direct dipole-dipole interaction between molecules can be important. For example, if the dipole-dipole Coulomb interaction between the molecules cannot be neglected, new collective modes emerge even in the absence of the nanophotonic cavity. These can be understood as collective density charge waves where the dipoles oscillate perpendicularly to the molecular plane with a characteristic pattern (i.e., a standing-wave-like pattern in the molecular plane with a characteristic in-plane wave vector resulting from the interference between the density waves due to reflection at the edges of the molecular patch); these are localized 2D phonon polaritons. One such collective mode is exemplified by the vertical lines in Fig. 1(b), with the length of each line illustrating the strength of the dipole associated with the vibration of the corresponding molecule collectively forming the stationary pattern.

To study the optical response of this system, we consider the Hamiltonian describing the interaction of one IR nanocavity mode with the ensemble of molecular vibrations, which also interact with each other,

$$\begin{aligned} \hat{H} &= \hat{H}_{\text{pht}} + \hat{H}_{\text{mol}} + \hat{H}_{\text{vib-pht}} + \hat{H}_{\text{vib-vib}} \\ &= \hbar\omega_{\text{cav}}\hat{a}^\dagger\hat{a} + \hbar\sum_{j=1}^N\omega_j\hat{b}_j^\dagger\hat{b}_j + \hbar\sum_{j=1}^Ng_j(\hat{a}^\dagger + \hat{a})(\hat{b}_j^\dagger + \hat{b}_j) \\ &\quad + \hbar\sum_j\sum_{l>j}\Omega_{jl}(\hat{b}_j^\dagger + \hat{b}_j)(\hat{b}_l^\dagger + \hat{b}_l), \end{aligned} \quad (1)$$

where  $\hat{a}$  and  $\hat{a}^\dagger$  are the bosonic annihilation and creation operators of the nanocavity excitations (e.g., plasmons or phonon polaritons), with frequency  $\omega_{\text{cav}}$ , respectively. The molecular vibrations at frequency  $\omega_j$  are quantized using the vibron (i.e., a quantum of intramolecular vibration) annihilation and creation operators  $\hat{b}_j$  and  $\hat{b}_j^\dagger$ , where the index  $j$  distinguishes between the molecules. Thus, the terms  $\hat{H}_{\text{pht}}$  and  $\hat{H}_{\text{mol}}$  in Eq. (1) correspond to the energy of the cavity mode and that of the vibrations, respectively. The third term  $\hat{H}_{\text{vib-pht}}$  describes the interaction between the vibration of each molecule and the IR cavity field mode, with coupling strength  $g_j$ . Here we specifically consider a nanocavity mode with a Gaussian field distribution [Fig. 1(b)]. Thus, for identical molecules the coupling strength is proportional to the cavity field,

$$g_j(\mathbf{r}_j) = g_0 \exp\left(-\frac{(x_j - x_0)^2 + (y_j - y_0)^2}{2\sigma_L^2}\right), \quad (2)$$

with  $|\mathbf{r}_j| = \sqrt{x_j^2 + y_j^2}$ ,  $g_0$  the value at the center  $\mathbf{r}_0 = (x_0, y_0)$  of this Gaussian function, and  $\sigma_L$  the standard deviation.

Finally,  $\hat{H}_{\text{vib-vib}}$  describes the intermolecular dipole-dipole interaction, where the coupling strength  $\hbar\Omega_{jl}$  between each pair of molecules  $j$  and  $l$  is given by the (static) Coulomb coupling as

$$\hbar\Omega_{jl} = \frac{1}{4\pi\epsilon_0 r_{jl}^3}[\mathbf{d}_j \cdot \mathbf{d}_l - 3(\mathbf{d}_j \cdot \mathbf{e}_{jl})(\mathbf{d}_l \cdot \mathbf{e}_{jl})]. \quad (3)$$

Here  $\mathbf{d}_j$  is the (real) transition dipole moment vector of molecule  $j$ ,  $\mathbf{r}_{jl}$  is the distance vector between molecules  $j$  and  $l$  (with  $\mathbf{e}_{jl}$  its unit vector),  $r_{jl} = |\mathbf{r}_{jl}|$ , and  $\epsilon_0$  is the vacuum permittivity.

We place the molecules in the  $xy$  plane, as described previously, and consider that all molecules have the same transition dipole moment  $\mathbf{d}_j \equiv \mathbf{d}_{\text{mol}}$  (aligned along the  $z$  axis) and the same bare energy  $\omega_j \equiv \omega_{\text{mol}}$ . In the following numerical calculations, we parametrize the interaction by considering the coupling between nearest neighbors,

$$\hbar\Omega_{jl}(r_{jl} = a) \equiv \hbar\Omega_0.$$

This model can be extended to different lattice configurations (including disordered ensembles), different dipole orientations, and samples where the molecules differ from each other.

Furthermore, note that we do not include a diamagnetic term  $\hat{H}_{\text{diam}} = \mathcal{D}(\hat{a}^\dagger + \hat{a})^2$ , which is often considered in ultra-strong coupling, where  $\mathcal{D} = \sum_j |g_j|^2/\omega_j$  [40]. The effect of this term on the diagonalization of the Hamiltonian can be reproduced by shifting the cavity frequency  $\omega'_{\text{cav}} \rightarrow \omega_{\text{cav}} + 2\mathcal{D}$

[41]. Thus, our conclusions should not be affected by the inclusion of this diamagnetic term.

### III. COLLECTIVE VIBRATIONAL STATES

In order to solve the full Hamiltonian of the system [Eq. (1)] and to better understand the emergence of collective vibrational modes, we first neglect the nanocavity mode and diagonalize the vibrational contribution to the Hamiltonian  $\hat{H}_{\text{coll}} = \hat{H}_{\text{mol}} + \hat{H}_{\text{vib-vib}}$ . Following the Bogoliubov procedure [42], there exist collective bosonic operators  $\hat{P}_n$  that are linear combinations of the vibrational operators  $\hat{b}_j$  of the individual molecules,

$$\hat{P}_n = \sum_{j=1}^N(\alpha_{nj}\hat{b}_j + \beta_{nj}\hat{b}_j^\dagger), \quad (4)$$

and diagonalize  $\hat{H}_{\text{coll}}$  according to

$$\hat{H}_{\text{coll}} = \hat{H}_{\text{mol}} + \hat{H}_{\text{vib-vib}} = \sum_n \hbar W_n \hat{P}_n^\dagger \hat{P}_n, \quad (5)$$

where  $\hat{P}_n$  and  $W_n$  are the new operators and eigenfrequencies of the collective modes of the system and  $[\hat{P}_n, \hat{H}_{\text{coll}}] = \hbar W_n \hat{P}_n$ . The subscript  $n$  refers to the index of the collective modes and  $j$  to the index of the molecules. To obtain the values of  $W_n$  and the  $\alpha_{nj}$  and  $\beta_{nj}$  coefficients, we write

$$[\hat{P}_n, \hat{H}_{\text{mol}} + \hat{H}_{\text{vib-vib}}] = \hbar W_n \hat{P}_n = \hbar W_n \sum_{j=1}^N(\alpha_{nj}\hat{b}_j + \beta_{nj}\hat{b}_j^\dagger). \quad (6)$$

From Eq. (4), the left-hand side of this expression is also

$$\begin{aligned} [\hat{P}_n, \hat{H}_{\text{mol}} + \hat{H}_{\text{vib-vib}}] &= \sum_j (\alpha_{nj}[\hat{b}_j, \hat{H}_{\text{vib}} + \hat{H}_{\text{vib-vib}}] \\ &\quad + \beta_{nj}[\hat{b}_j^\dagger, \hat{H}_{\text{vib}} + \hat{H}_{\text{vib-vib}}]). \end{aligned} \quad (7)$$

Inserting the expression for  $\hat{H}_{\text{mol}} + \hat{H}_{\text{vib-vib}}$  given by Eq. (1) into the right-hand side of Eq. (7) and comparing the resulting equations with Eq. (6), we obtain a system of linear equations resulting in the eigenvalue problem  $\mathbf{M}\mathbf{V}_n = W_n\mathbf{V}_n$ , where  $\mathbf{M}$  is the Hopfield matrix [43]

$$\mathbf{M} = \begin{pmatrix} \omega_1 & 0 & \Omega_{12} & -\Omega_{12} & \dots & \Omega_{1N} & -\Omega_{1N} \\ 0 & -\omega_1 & \Omega_{12} & -\Omega_{12} & \dots & \Omega_{1N} & -\Omega_{1N} \\ \Omega_{12} & -\Omega_{12} & \omega_2 & 0 & \dots & \Omega_{2N} & -\Omega_{2N} \\ \Omega_{12} & -\Omega_{12} & 0 & -\omega_2 & \dots & \Omega_{2N} & -\Omega_{2N} \\ \vdots & \vdots & \vdots & \vdots & \ddots & \vdots & \vdots \\ \Omega_{1N} & -\Omega_{1N} & \Omega_{2N} & -\Omega_{2N} & \dots & \omega_N & 0 \\ \Omega_{1N} & -\Omega_{1N} & \Omega_{2N} & -\Omega_{2N} & \dots & 0 & -\omega_N \end{pmatrix}_{2N \times 2N}. \quad (8)$$

This matrix admits  $2N$  eigenvalues, and if  $W_n$  is an eigenvalue, so is  $-W_n$ . The  $N$  distinct frequencies  $W_n$  correspond to the normal modes, i.e., the collective states. The eigenvectors  $\mathbf{V}_n$  are determined by the values of  $\alpha_{nj}$  and  $\beta_{nj}$ ,

$$\mathbf{V}_n^T = (\alpha_{n1} \quad \beta_{n1} \quad \dots \quad \alpha_{nN} \quad \beta_{nN})_{1 \times 2N}, \quad (9)$$

where  $\sum_{j=1}^N(|\alpha_{nj}|^2 - |\beta_{nj}|^2) = 1$  ensures the bosonicity of the operators. The matrix  $\mathbf{M}$  is real and block symmetric.

Not all matrices  $\mathbf{M}$  show exclusively real eigenvalues. However, for the parameters we consider, we find real eigenvalues and eigenvectors. Since the vector elements of  $\mathbf{V}_n$  are real (i.e.,  $\alpha_{nj}^* = \alpha_{nj}$  and  $\beta_{nj}^* = \beta_{nj}$ ), we can write, from Eq. (4),

$$\hat{P}_n^\dagger + \hat{P}_n = \sum_{j=1}^N (\alpha_{nj} + \beta_{nj}) (\hat{b}_j^\dagger + \hat{b}_j),$$

which can be written as a matrix-vector product. Inverting this matrix allows us to write  $\hat{b}_j^\dagger + \hat{b}_j$  as a function of  $\hat{P}_n^\dagger + \hat{P}_n$ . Defining the  $N \times N$  inverse matrix  $X_{jn} = (\alpha_{nj} + \beta_{nj})^{-1}$  [44], we obtain

$$(\hat{b}_j^\dagger + \hat{b}_j) = \sum_n X_{jn} (\hat{P}_n^\dagger + \hat{P}_n). \quad (10)$$

### Analysis of the new collective vibrational modes

We show the nature of some illustrative collective modes in Figs. 2(a)–2(d) for the  $N = 51 \times 51 = 2601$  molecules in a square lattice. In this paper we do not consider any change of the interaction at edges; only the number of neighbors differs. We set the nearest-neighbor interaction strength to  $\hbar\Omega_0 = 1$  meV and indicate above each panel the corresponding eigenenergy  $W_n$  of the mode  $n$ . The value of  $\Omega_0$  is chosen to be comparable to the value for van der Waals or other polar materials (see Appendix A). Each panel represents the spatial pattern of the eigenvalue associated with the collective mode, which is plotted as a color plot of the amplitude of the  $\alpha_{nj}$  coefficients (with each  $\alpha_{nj}$  corresponding to a molecule  $j$ ) as a function of the location of the molecules in the  $xy$  plane. We observe that the collective mode with the largest energy [Fig. 2(a)] corresponds to all molecules oscillating in phase (same sign), while other modes show approximately periodic changes of sign of the individual vibrational amplitudes in the  $x$  and  $y$  directions. Thus, the collective modes can be thought of as the standing-wave pattern of a density wave of molecular vibrations (oscillating in the  $z$  direction) with a characteristic in-plane wave vector along the  $xy$  plane of the 2D molecular monolayer. The position of these collective modes in the energy dispersion relation of the molecular layer is marked with purple circles in Fig. 2(e).

To understand the coupling of the collective mode  $n$  with light, it is useful to obtain the dipole moment of the collective mode  $\mathbf{D}_n$ , as only modes with a significant value of  $\mathbf{D}_n$  couple efficiently, in the absence of nanocavity, with an incoming laser or other focused illumination (characterized by almost constant fields in the molecular ensemble). The total dipole can be written in terms of the operators of each molecule as  $\hat{D} = \sum_{j=1}^N \mathbf{d}_j (\hat{b}_j^\dagger + \hat{b}_j)$ . Transforming to the collective picture, we can write

$$\hat{D} = \sum_{j=1}^N X_{jn} \mathbf{d}_j (\hat{P}_n^\dagger + \hat{P}_n). \quad (11)$$

We find that the collective mode with higher energy shows the highest nonzero total dipole moment  $\mathbf{D}_1 = \sum_{j=1}^N \mathbf{d}_j X_{j1} = 43.72 \mathbf{d}_{\text{mol}}$ . This efficient coupling in this mode can be expected because the induced molecular dipoles oscillate with the same phase, as mentioned previously. Lower-energy eigenvalues have generally much lower values of  $\mathbf{D}_n$  due

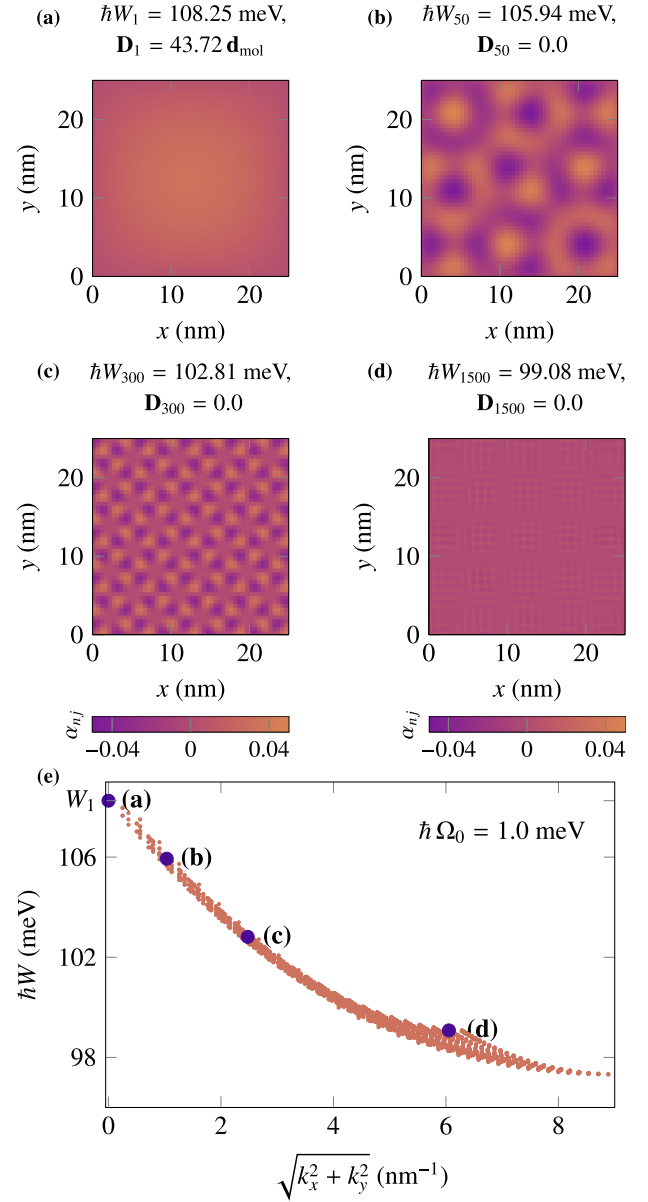


FIG. 2. Eigenmodes and eigenenergies of a molecular layer in the absence of nanocavity, for  $N = 51 \times 51 = 2601$  molecules arranged in a 2D square lattice. (a)–(d) Collective vibrational modes arising from dipole-dipole interactions. The color plot shows the distribution of the values of the coefficient  $\alpha_{nj}$  of the system eigenvectors in the  $xy$  plane for the collective modes (a)  $n = 1$ , (b)  $n = 50$ , (c)  $n = 300$ , and (d)  $n = 1500$  [marked by the purple circles in (e)]. Each  $\alpha_{nj}$  is associated with a molecule and thus with a spatial position. For each mode, we also indicate the corresponding eigenfrequency  $W_n$  and total dipole moment  $\mathbf{D}_n$ . (e) Dispersion relation, corresponding to the energy of the modes of the system, plotted as a function of the wave vector  $|\mathbf{k}| = \sqrt{k_x^2 + k_y^2}$  associated with each eigenvector. In (a)–(e) we use lattice constant  $a = 0.5$  nm, dipole-dipole interaction  $\hbar\Omega_0 = 1$  meV, and vibrational energy  $\hbar\omega_{\text{mol}} = 100$  meV.

to the sign changes of  $\alpha_{nj}(\beta_{nj})$  and thus are more difficult to excite optically. For example, the low-energy modes in Figs. 2(b)–2(d) are characterized by  $\mathbf{D}_n = 0$ . To further characterize the collective modes and based on the clear

periodicity of the vibrational pattern in Figs. 2(a)–2(d), we calculate for each mode  $n$  the 2D Fourier transform of the spatial  $\alpha_{nj}$  maps in the  $xy$  plane,  $|\mathcal{F}[\alpha_{nj}]|^2$ . We then define the characteristic wave vector of each mode,  $k_{x,y}$ , where  $k_x$  and  $k_y$  are the wave-vector components on the  $x$  and  $y$  axes, respectively, as the value at which the corresponding maximum of  $|\mathcal{F}[\alpha_{nj}]|^2$  is found. In Fig. 2(e) we present the resulting dispersion relation, showing the energy of the modes as a function of the parallel wave vector  $\sqrt{k_x^2 + k_y^2}$ . This dispersion follows closely that of an infinite 2D layer of identical molecules, as shown in Appendix C. We find that the energies cover a frequency range between 97.32 and 108.25 meV. The results show a certain spreading of the data points, i.e., modes can have the same  $\sqrt{(k_x^{\max})^2 + (k_y^{\max})^2}$  but a different energy because the square lattice is not isotropic, so the direction in the  $(k_x, k_y)$  plane influences the result, particularly for large  $\sqrt{(k_x^{\max})^2 + (k_y^{\max})^2}$ . Specifically, the obtained values are contained within an upper set of points corresponding to  $k_y(k_x) = 0$  that reaches  $k_x^{\max}(k_y^{\max}) = \pi/a \sim 6.28 \text{ nm}^{-1}$  and a lower one for  $k_x^{\max} = k_y^{\max}$  that reaches  $\sqrt{(k_x^{\max})^2 + (k_y^{\max})^2} = \sqrt{2}(\pi/a) \sim 8.89 \text{ nm}^{-1}$  (see further discussion in Appendix C). As for our particular example we have chosen to orientate the dipole moments in the direction perpendicular to the  $xy$  plane where the molecules are situated, the modes of smaller wave vectors are characterized by larger energies.

#### IV. COLLECTIVE VIBRATIONAL DYNAMICS OF A MOLECULAR MONOLAYER COUPLED TO A CAVITY

We consider next the effect of the coupling of the molecules with the nanophotonic mode. With this purpose, we return to the total Hamiltonian in Eq. (1) and use Eq. (10) to rewrite

$$\hat{H}_{\text{vib-pht}} = \hbar \sum_j g_j (\hat{a}^\dagger + \hat{a})(\hat{b}_j^\dagger + \hat{b}_j) \quad (12)$$

in terms of the collective operators, which gives

$$\begin{aligned} \hat{H}_{\text{pht-coll}} &= \hbar \sum_n \sum_j g_j X_{jn} (\hat{a}^\dagger + \hat{a})(\hat{P}_n^\dagger + \hat{P}_n) \\ &= \hbar \sum_n \mathcal{G}_n (\hat{a}^\dagger + \hat{a})(\hat{P}_n^\dagger + \hat{P}_n), \end{aligned} \quad (13)$$

where we defined  $\mathcal{G}_n = \sum_j g_j X_{jn}$ . Thus, in the new collective base

$$\begin{aligned} \hat{H} &= \hbar \omega_{\text{cav}} \hat{a}^\dagger \hat{a} + \hbar \sum_n W_n \hat{P}_n^\dagger \hat{P}_n \\ &+ \hbar (\hat{a}^\dagger + \hat{a}) \sum_n \mathcal{G}_n (\hat{P}_n^\dagger + \hat{P}_n). \end{aligned} \quad (14)$$

A photonic nanocavity mode characterized by homogeneous fields couples preferentially with the largest-energy mode due to its particularly large dipole strength (and the large resulting  $\mathcal{G}_n$ ). Thus, it is informative to diagonalize the Hamiltonian in the simple case that just one collective state of frequency  $W$  interacts with one cavity mode. We look for the two new polariton operators  $\hat{q}_m = \zeta_{m1} \hat{a} +$

$\eta_{m1} \hat{a}^\dagger + \zeta_{m2} \hat{P} + \eta_{m2} \hat{P}^\dagger$ , where the Hopfield coefficients  $\zeta_{lm}$  and  $\eta_{lm}$  ( $l, m = 1, 2$ ) satisfy the normalization condition  $|\zeta_{l1}|^2 - |\eta_{l1}|^2 + |\zeta_{l2}|^2 - |\eta_{l2}|^2 = 1$ . Following a Bogoliubov diagonalization procedure [42], the characteristic polynomial of the eigenproblem [ $\det(\mathbf{I}\mathcal{W} - \mathbf{M}) = 0$ ] can be written as

$$(\omega_{\text{cav}}^2 - \mathcal{W}^2)(W_1^2 - \mathcal{W}^2) - 4\omega_{\text{cav}} W_1 \mathcal{G}_1^2 = 0. \quad (15)$$

The solutions of this equation are the eigenenergies of the two vibron-polariton modes [20]

$$\mathcal{W}_\pm^2 = \frac{1}{2} [\omega_{\text{cav}}^2 + W_1^2 \pm \sqrt{(\omega_{\text{cav}}^2 - W_1^2)^2 + 16\mathcal{G}_1^2 \omega_{\text{cav}} W_1}]. \quad (16)$$

which indicates that the new modes are separated by an energy difference that depends on the coupling strength  $\mathcal{G}_1$  and on the cavity detuning. Equation (16) is formally equivalent to the equation obtained for coupling between a single molecular vibration and a cavity mode [21,45] [note that Eq. (16) slightly differs from the expression that is found when the rotating-wave approximation is used]. The main aspects to consider when coupling with a collective mode are that (i)  $W_1$  in Eq. (16) corresponds to the frequency of the collective vibrational mode (without cavity) and not to the resonant frequency of the individual molecules, (ii) the coupling strength  $\mathcal{G}_1$  includes a contribution from all molecules that couple with the photonic nanocavity [46,47], and (iii) together with the two bright modes at energies  $\mathcal{W}_\pm$ , there are  $N - 1$  dark modes that do not couple at all with the cavity in this approximation [24,48,49].

We consider next the general case where the nanophotonic cavity field can be strongly inhomogeneous, and we need to consider all the collective modes simultaneously. The  $N + 1$  eigenfrequencies  $\mathcal{W}_m$  and eigenvectors  $(\zeta_{m1} \ \eta_{m1} \ \zeta_{m2} \ \eta_{m2} \ \dots)^T$  of the system can be found by diagonalizing the matrix

$$\mathbf{M} = \begin{pmatrix} \omega_{\text{cav}} & 0 & \mathcal{G}_1 & -\mathcal{G}_1 & \mathcal{G}_M & -\mathcal{G}_M \\ 0 & -\omega_{\text{cav}} & \mathcal{G}_1 & -\mathcal{G}_1 & \dots & \mathcal{G}_M & -\mathcal{G}_M \\ \mathcal{G}_1 & -\mathcal{G}_1 & W_1 & 0 & \dots & 0 & 0 \\ \mathcal{G}_1 & -\mathcal{G}_1 & 0 & -W_1 & \dots & 0 & 0 \\ \vdots & \vdots & \vdots & \vdots & \ddots & \vdots & \vdots \\ \mathcal{G}_M & -\mathcal{G}_M & 0 & 0 & \dots & W_M & 0 \\ \mathcal{G}_M & -\mathcal{G}_M & 0 & 0 & \dots & 0 & -W_M \end{pmatrix}, \quad (17)$$

which results in the transformed Hamiltonian  $\hat{H} = \sum_{m=1}^M \hbar \mathcal{W}_m \hat{q}_m^\dagger \hat{q}_m$ , where  $M = N + 1$ .

To analyze the optical response of the system, we consider the typical situation where the optical dipole of the nanophotonic cavity is much larger than that of the molecules (or, in an alternative picture, that the field induced by the nanophotonic cavity is much larger than the incident field). Thus, the coupling of light with the system is mostly dominated by the photonic fraction of each mode  $m$ , which is given by  $|\zeta_{m1}|^2 - |\eta_{m1}|^2$ . We then define the spectral function

$$S(\omega) = \sum_m (|\zeta_{m1}|^2 - |\eta_{m1}|^2) \frac{\gamma/2}{(\omega - \mathcal{W}_m)^2 + (\gamma/2)^2} \quad (18)$$

to characterize the optical response of the system, where we include *ad hoc* the effect of losses through the damping rate  $\gamma$ , which were neglected in the original Hamiltonian, converting the  $\delta$ -like modes to Lorentzians. We set the losses to  $\hbar\gamma = 1$  meV except when explicitly stated otherwise. For simplicity, Eq. (18) does not consider interference effects between different modes that could induce Fano resonances under certain experimental conditions [10,50,51]. In Appendix D we discuss how, for the systems considered here, introducing losses in this way gives almost identical results as including complex-value (lossy) frequencies in the Hamiltonian.

### A. Optical response of the vibrational modes

For the following analysis, we study the effect of separately changing the different parameters: the strength of the dipole-dipole interaction  $\Omega_0$ , the confinement  $\sigma_L$ , the molecule-cavity strength  $g_{\text{tot}}$ , and the losses  $\gamma$ . Other possibilities, such as modifying the lattice parameter  $a$ , can be thought of as a combination of these separate changes (see more details in Appendix B).

We consider as a first step a nanophotonic cavity characterized by a homogenous field distribution ( $\sigma_L \rightarrow \infty$ ), which couples with the 2D molecular square patch containing  $N = 51 \times 51 = 2601$  molecules that was analyzed in Sec. III. The optical spectrum of the system is shown in Fig. 3(a) as a function of the frequency of the cavity  $\omega_{\text{cav}}$  for the case of no direct molecule-molecule coupling  $\Omega_0 = 0$  and molecule-cavity coupling strength  $\hbar g_j(\mathbf{r}_j) \approx 0.04$  meV [throughout the paper we set  $\hbar g_{\text{tot}} = \hbar \sqrt{\sum_j |g_j(\mathbf{r}_j)|^2}$ , except when explicitly stated otherwise]. For large detuning  $\omega_{\text{cav}} - \omega_{\text{mol}}$ , we observe a single peak at the frequency of the nanophotonic mode. As  $\omega_{\text{cav}} \rightarrow \omega_{\text{mol}}$ , the second mode becomes visible and the two peaks show the typical avoided anticrossing.

This avoided anticrossing is a characteristic property of the strong-coupling regime [52,53] and can be described by setting the dipole-dipole interaction to zero  $\Omega_{jl} = 0$  and  $\omega_j = \omega_{\text{mol}}$  in Eq. (1) and defining  $N$  new operators  $\hat{S}_j = \sum_{l=1}^N c_{jl} \hat{b}_l$ , where  $c_{jl}$  are coefficients forming an orthonormal base and  $(c_{11}, c_{12}, \dots, c_{1N}) = (g_1, g_2, \dots, g_N) / \sqrt{\sum_{j=1}^N |g_j|^2}$  [48]. Then  $\hat{S}_1$  is the only collective mode coupled to the cavity, with a total effective coupling

$$g_{\text{tot}} = \sqrt{\sum_{j=1}^N |g_j|^2},$$

thus allowing us to write

$$\hat{H}_{\text{coll}} = \hbar \omega_{\text{cav}} \hat{a}^\dagger \hat{a} + \hbar \sum_{j=1}^N \omega_{\text{mol}} \hat{S}_j^\dagger \hat{S}_j + \hbar g_{\text{tot}} (\hat{a}^\dagger + \hat{a}) (\hat{S}_1^\dagger + \hat{S}_1). \quad (19)$$

Figure 3 shows the results for  $\hbar g_{\text{tot}} = 2$  meV. This Hamiltonian has  $N + 1$  excited eigenstates: two polariton modes, with eigenfrequencies approximately equal to  $\omega_{\text{mol}} \pm g_{\text{tot}}$  (resulting from the linear combination of the cavity mode and the collective bright state of the molecules), and  $N - 1$  dark modes that do not couple with the nanophotonic cavity (these dark modes are combinations of molecular excitations orthogonal to the

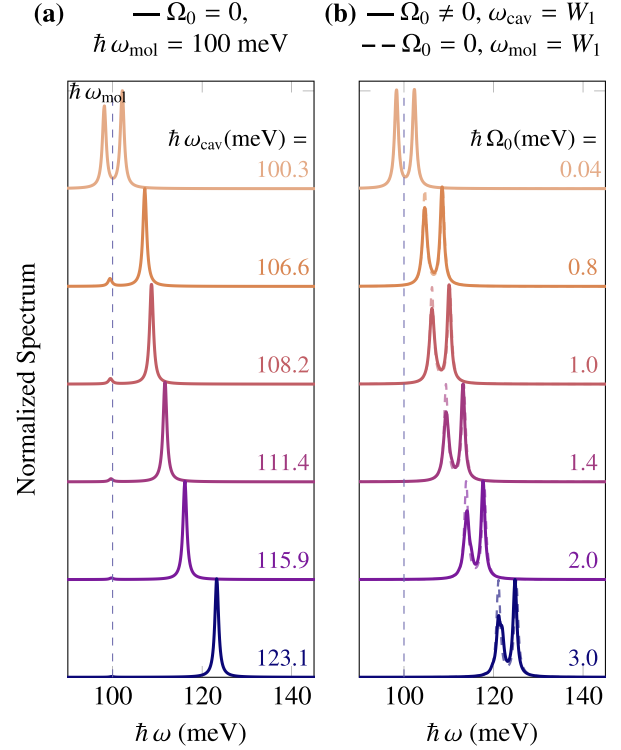


FIG. 3. Effect of direct molecule-molecule coupling on the optical spectrum  $S(\omega)$  of a spatially homogeneous IR cavity mode coupled to a 2D square lattice with  $N = 51 \times 51 = 2601$  molecules. The solid lines correspond to the normalized spectrum (a) ignoring ( $\Omega_0 = 0$ ) and (b) including the molecule-molecule interaction ( $\Omega_0 \neq 0$ ), with the resonant frequency of the molecule set to  $\hbar\omega_{\text{mol}} = 100$  meV (highlighted by the light blue vertical dashed lines). In (a) different spectra (shifted vertically for visibility) correspond to different frequencies of the cavity modes  $\omega_{\text{cav}}$ . In (b) the same  $\omega_{\text{cav}}$  are considered and the dipole-dipole coupling strength  $\Omega_0$  is changed between spectra. The  $\Omega_0$  values are chosen so that, for each spectrum, the maximum frequency of the collective eigenmodes, i.e.,  $W_1$ , corresponding to the collective mode with associated wave vector  $\mathbf{k} = 0$  in Figs. 2(a) and 2(e), is equal to the cavity frequency. This condition corresponds to resonant coupling. The dashed lines in (b) correspond to the spectra obtained without the molecule-molecule interaction but setting  $\omega_{\text{mol}} = W_1$ , i.e., the frequency of the  $\mathbf{k} = 0$  collective mode that would be obtained if the molecule-molecule interaction were included. The results are obtained for a homogeneous field distribution  $\hbar g_j(\mathbf{r}_j) \approx 0.04$  meV, lattice constant  $a = 0.5$  nm, total molecule-cavity coupling strength  $\hbar g_{\text{tot}} = \hbar \sqrt{\sum_j |g_j(\mathbf{r}_j)|^2} = 2$  meV, and  $\hbar\gamma = 1$  meV.

collective bright state of the molecular excitation) [24,49]. The exact expression (for no losses) of the eigenfrequencies of the polaritonic modes is given by Eq. (16) after changing  $W \rightarrow \omega_{\text{mol}}$  and the effective coupling strength to  $\mathcal{G}_1 \rightarrow g_{\text{tot}}$ .

The spectral response after switching on the molecule-molecule coupling,  $\Omega_0 \neq 0$ , is shown by the solid lines in Fig. 3(b) for the same  $\omega_{\text{cav}}$  values (we use a different value of  $\Omega_0 > 0$  for each value of the cavity resonance, as indicated by the labels, for reasons explained below; since  $\Omega_0$  is defined in units of energy, changing its value could be seen as changing  $a$  while keeping the dipole moment unchanged, or vice versa). In this case,  $\omega_{\text{cav}}, \Omega_0 > 0$  and we observe two closely situated

peaks for all  $\omega_{\text{cav}}$ , which is drastically different from the results for the equivalent situation with  $\Omega_0 = 0$  (and the same values of  $\omega_{\text{cav}}$ ). This difference can be connected to the dispersion of the collective modes for nonzero molecule-molecule coupling (Fig. 2). The coupling with a cavity mode characterized by homogenous fields is dominated by the collective vibrational excitations of small wave vector  $|\mathbf{k}| = \sqrt{k_x^2 + k_y^2}$ , whose eigenenergies are significantly larger than the molecular one. The energy of the excitations that couple with the cavity are thus very different depending on whether the direct molecule-molecule coupling is included or not.

To take into account the shift from the molecular vibrational energy to the energy of the brightest collective mode, we also perform simulations where no molecule-molecule interactions are considered but setting the molecular frequency to  $\omega_{\text{mol}} = W_1$ . Here  $W_1$  corresponds to the maximum frequency in the dispersion, associated with the collective mode characterized by  $\mathbf{k} = 0$  ( $W_1$  is obtained for the values of  $\Omega_0$  indicated by the labels, but the molecule-molecule interaction term in the Hamiltonian is not included in the calculation of the spectra). The obtained results are shown by the dashed lines in Fig. 3(b) and are generally very similar to the results in Fig. 3(b) with dipole-dipole interaction (and unshifted vibrational frequency  $\hbar\omega_{\text{mol}} = 100$  meV), plotted with solid lines. Further, we note that the values of  $\Omega_0$  for each cavity frequency  $\omega_{\text{cav}}$  are chosen in Fig. 3(b) so that  $W_1 = \omega_{\text{cav}}$  (resonant system), which explains why we always obtain two peaks of similar amplitude.

The results in Fig. 3(b) thus indicate that the molecule-molecule interaction can strongly modify the optical response but that, for a spatially homogenous cavity field, this effect can be mostly corrected by considering a shifted vibrational frequency  $\omega_{\text{mol}} \rightarrow W_1$ . Shifts from the bare molecular frequencies in optical spectra due to dipole-dipole interactions can also occur in  $J$ -aggregate ensembles [54] and absorbed molecules [55].

From a practical perspective, this renormalization of the energy can be accomplished by associating the vibrational frequency with the resonance of the classical permittivity of the infinite material (monolayer in the case in this work), as, to a first approximation, the classical permittivity is a response function that already contains the interactions between different regions of the material (via a Clausius-Mossotti-like relation, for instance). This approach was followed, for example, in Ref. [26].

We emphasize further the energy renormalization in Fig. 4(a), where we plot the results over a smaller frequency range for different effective coupling strength  $g_{\text{tot}} = \sqrt{\sum_{j=1}^N |g_j(\mathbf{r})|^2}$ . In this case, we include a weak variation of the spatial field distribution of the photonic mode ( $\sigma_L = 15a$ ) and the system is in resonance  $\hbar\omega_{\text{cav}} = \hbar W_1 \approx 108.2$  meV. Consistent with the results in Fig. 3, the results obtained including the molecule-molecule interactions ( $\hbar\Omega_0 = 1$  meV and using the vibrational frequency  $\omega_{\text{mol}}$  (solid lines) are very similar to those obtained for  $\Omega_0 = 0$  and  $\hbar\omega_{\text{mol}} = \hbar W_1 \approx 108.2$  meV. All spectra show two almost symmetric peaks, with energy separation (Rabi splitting) that increases with growing  $g_{\text{tot}}$ . In contrast, the direct molecule-molecule interactions can strongly modify the optical spectra for a tightly

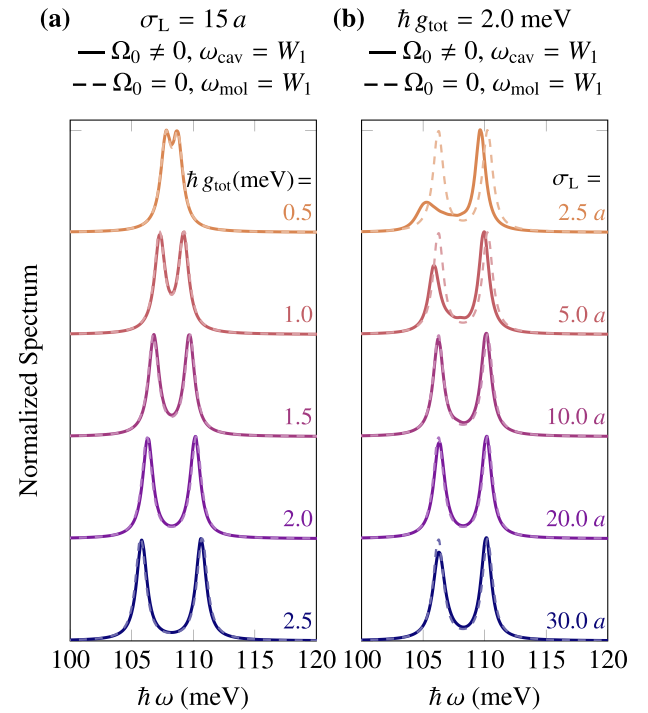


FIG. 4. Influence of the direct dipole-dipole interactions on the optical spectra  $S(\omega)$  for different values of the coupling strength and field localization. The normalized optical spectra of an IR cavity coupled to a 2D square lattice with  $N = 51 \times 51 = 2601$  molecules is plotted (a) changing the total molecule-cavity coupling strength  $g_{\text{tot}}^2 = \sum_j |g_j(\mathbf{r})|^2$  (values indicated in the figure) while keeping fixed the width of the field distribution to  $\sigma_L = 15a$  and (b) changing the field localization of the photonic mode  $\sigma_L$  (values indicated in the figure) and keeping  $\hbar g_{\text{tot}} = 2$  meV fixed. Solid lines correspond to the results obtained including direct molecule-molecule interactions with  $\hbar\Omega_0 = 1$  meV and vibrational frequency  $\hbar\omega_{\text{mol}} = 100$  meV. Dashed lines represent the values without molecule-molecule interactions and using  $\hbar\omega_{\text{mol}} = \hbar W_1 \approx 108.2$  meV. We also set  $\hbar\omega_{\text{cav}} = \hbar W_1 \approx 108.2$  meV for all spectra. The spectra are shifted vertically for visibility and are obtained for lattice constant  $a = 0.5$  nm. We set  $\hbar\gamma = 1$  meV.

confined cavity field. This effect is illustrated in Fig. 4(b), where we fix  $\hbar g_{\text{tot}} = 2$  meV and vary the field confinement  $\sigma_L/a$ . The cavity resonance is again chosen to be resonant with  $W_1$ . The constant value of  $g_{\text{tot}}$  assumed in this case implies a strengthening of the coupling of the cavity with each individual molecule  $g_j$  for increased field confinement (smaller  $\sigma_L/a$ ), as the number of molecules interacting with the cavity field is effectively reduced. We observe that, for  $\sigma_L/a \lesssim 5$ , there is a striking difference between the results obtained including molecule-molecule interactions ( $\hbar\Omega_0 = 1$  meV and  $\hbar\omega_{\text{mol}} = 100$  meV, solid line) and those without these interactions ( $\Omega_0 = 0$  and  $\hbar\omega_{\text{mol}} = \hbar W_1 \approx 108.2$  meV, dashed line). The former shows a gradual smearing out and disappearance of the low-energy peak that is not present for the latter, a behavior that can be understood from the following simple picture. A weakly confined (i.e., almost uniform) nanocavity field couples preferentially with the single eigenmode at  $\sqrt{k_x^2 + k_y^2} = 0$  that is characterized by a significantly larger dipole moment  $\sum_j X_{jn} \mathbf{d}_{\text{mol}}$  than that of the

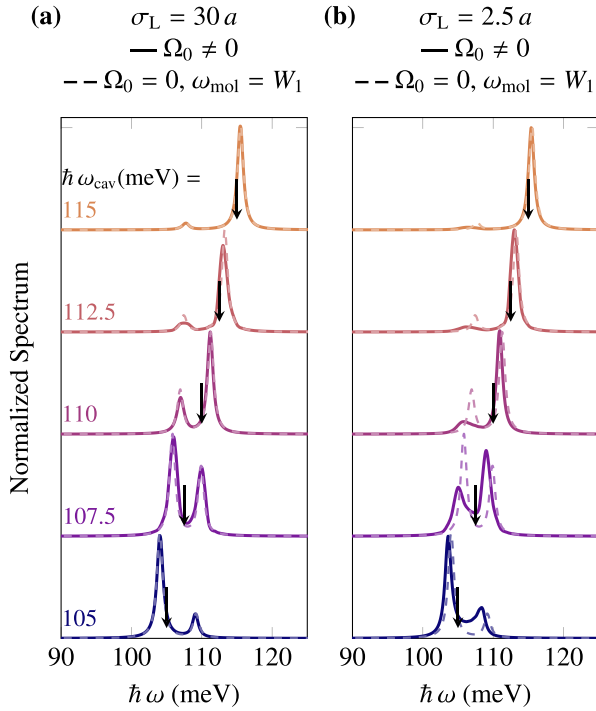


FIG. 5. Influence of direct molecule-molecule interactions for different cavity frequencies of an IR cavity characterized by (a) an almost homogeneous and (b) an inhomogeneous field distribution. The cavity is coupled to a 2D square lattice with  $N = 51 \times 51 = 2601$  molecules and the normalized optical spectrum is plotted for different cavity frequencies, indicated in the figure (arrows) and including (solid lines) or ignoring (dashed lines) direct molecule-molecule interactions. The former considers vibrational energy  $\hbar\omega_{\text{mol}} = 100$  meV and the latter  $\hbar\omega_{\text{mol}} = \hbar W_1 \approx 108.2$  meV. The spectra are shifted vertically for visibility and are obtained for a field distribution of width (a)  $\sigma_L = 30a$  and (b)  $\sigma_L = 2.5a$ . The other parameters are the dipole-dipole coupling strength  $\hbar\Omega_0 = 1$  meV, lattice constant  $a = 0.5$  nm, total molecule-cavity coupling strength  $\hbar g_{\text{tot}} = \hbar \sqrt{\sum_j |g_j(\mathbf{r})|^2} = 2$  meV, and  $\hbar\gamma = 1$  meV.

other eigenvalues. Thus, the optical response is dominated by the coupling between the photonic mode and one collective vibrational mode, resulting in the standard emergence of two almost symmetric peaks of a typical strongly coupled resonant system [see Eqs. (16) and (19)]. On the other hand, a strongly confined field can couple efficiently (large  $\mathcal{G}_n$ ) with modes of higher order (larger  $\sqrt{k_x^2 + k_y^2}$ ), resulting in a more complex spectrum with contributions from many collective vibrational modes along the dispersion curve. As a subtle point, we note that the difference between the two spectra (with and without molecule-molecule interactions) is smallest for  $\sigma_L/a \approx 10$ – $20$  and it increases for less confined fields (larger  $\sigma_L/a$ ), which we attribute to the illumination of the molecules near the edges of the molecular ensemble. However, the differences in this case of almost homogeneous fields remain significantly smaller than in the case of very strongly confined fields.

We confirm the importance of direct molecule-molecule interactions for strong nanocavity field confinement by showing in Fig. 5 the optical spectra as a function of the frequency of the cavity mode  $\omega_{\text{cav}}$ . We consider a small [ $\sigma_L = 30a$ ,

Fig. 5(a)] and a large [ $\sigma_L = 2.5a$ , Fig. 5(b)] field confinement and the other parameters are kept the same as in Fig. 4(b) both when including (solid lines) and neglecting (dashed lines) the direct molecule-molecule interactions. In all cases, we find the typical avoided-crossing near-resonant conditions ( $\hbar\omega_{\text{cav}} \approx \hbar W_1 \approx 108.2$  meV). Further, for weak-field confinement, we find very similar results independently of the inclusion or exclusion of the direct molecule-molecule interaction. In contrast, for the strongly confined nanocavity field, including the direct interaction [solid line in Fig. 5(b)] strongly affects the results: By comparison, the peak spectrally closer to  $\omega_{\text{mol}} = W_1$  becomes weaker and broader than the one near  $\omega_{\text{cav}}$  (or the ones with no direct-direct interaction).

### B. Establishing the criteria for strong dipole-dipole interaction

We focus next on determining the condition that needs to be fulfilled for the direct molecule-molecule interactions to change significantly the optical response of a coupled system beyond a simple energy renormalization. With this purpose, we first consider that the cavity field mostly extends over a range approximately equal to  $[0, k_{\text{max}}]$  of wave vectors in  $k$  space. This range of wave vectors would indicate the set of modes from the dispersion [Fig. 2(e)] of the 2D material that can be excited. The numerical dispersion for small  $\mathbf{k}$  can be approximated by (see derivation in Appendix C)

$$\omega(\mathbf{k}) = \sqrt{\omega_{\text{mol}}^2 + 2\omega_{\text{mol}} \sum_{m,n} \frac{\Omega_0}{(\sqrt{m^2 + n^2})^3}} - 2\pi\Omega_0|\mathbf{k}|a \quad (20)$$

(the sum runs over  $m, n = -N/2$  to  $N/2$ , excluding  $n = m$ ) so that the range of wave vectors approximately equal to  $[0, |\mathbf{k}_{\text{max}}|]$  corresponds to frequencies covering a spectral width  $\Delta\omega = \omega_{\text{max}} - \omega_{\text{min}} = 2\pi\Omega_0|\mathbf{k}_{\text{max}}|a$ . We propose that the molecule-molecule interactions need to be considered explicitly in the Hamiltonian when this spectral width is of the order of or larger than the losses, i.e.,  $\Delta\omega \gtrsim \gamma$ , corresponding to the following condition:

$$2\pi\Omega_0 \frac{a}{\sigma_L} \gtrsim \gamma. \quad (21)$$

We have approximated  $|\mathbf{k}_{\text{max}}| \approx 1/\sigma_L$  for the Gaussian illumination of width (in real space)  $\sigma_L$ . Equation (21) predicts that the direct molecule-molecule interaction needs to be included in the Hamiltonian for very large coupling strength, very large confinement (low  $\sigma_L$ ), and/or very low losses. This equation could be further generalized to other conditions, such as different illuminations. This criterion depends only on the ratio of the different parameters  $\sigma_L/a$  and  $\Omega_0/\gamma$ , not on their absolute value.

To assess the validity of the proposed equation, we first consider a particular example of dipole-dipole coupling strength  $\hbar\Omega_0 = 1$  meV,  $\sigma_L = 2.5a$  and optical coupling strength  $\hbar g_{\text{tot}} = 1$  meV. Figure 6 shows the corresponding spectra as the loss varies  $\gamma$ , again including the dipole-dipole interactions in the Hamiltonian and setting  $\hbar\omega_{\text{mol}} = 100$  meV (solid line) or ignoring them and renormalizing the vibrational energy to  $\omega_{\text{mol}} = W_1$  (dashed line). We observe that the two spectra start to differ for  $\hbar\gamma \lesssim 2$ – $3$  meV, consistent with the condition  $\hbar\gamma \lesssim 2.5$  meV obtained from Eq. (21). Interestingly, the spectrum obtained for the weakest losses



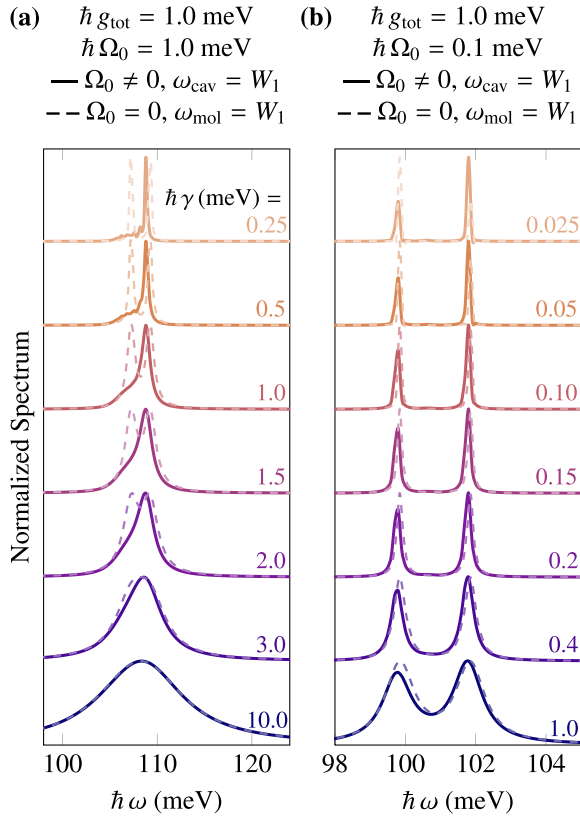


FIG. 6. Influence of losses  $\gamma$  in the normalized spectrum. The cavity is coupled to a 2D square lattice with  $N = 51 \times 51 = 2601$  molecules and the normalized optical spectrum is plotted for different cavity losses  $\gamma$ , indicated in the figure, and including (solid lines) or ignoring (dashed lines) direct molecule-molecule interactions. The former considers vibrational energy  $\hbar\omega_{\text{mol}} = 100$  meV and the latter  $\omega_{\text{mol}} = W_1$ . The spectra are shifted vertically for visibility and are obtained for a field distribution of width  $\sigma_L = 2.5a$ . The other parameters are the dipole-dipole coupling strength (a)  $\hbar\Omega_0 = 1$  meV ( $\hbar W_1 \approx 108.2$  meV) and (b)  $\hbar\Omega_0 = 0.1$  meV ( $\hbar W_1 \approx 100.8$  meV) as well as  $\omega_{\text{cav}} = W_1$ , lattice constant  $a = 0.5$  nm, and total molecule-cavity coupling strength  $\hbar\sqrt{\sum_j |g_j(\mathbf{r})|^2} = 1$  meV.

( $\hbar\gamma = 0.25$  meV) and including dipole-dipole interactions shows many small narrow peaks, a direct signature of the participation of more than one collective vibrational mode in the response.

As the threshold condition of  $\gamma$  scales directly with  $\Omega_0$ , we next perform in Fig. 6(b) a similar analysis for a much smaller value of the dipole-dipole interactions,  $\hbar\Omega_0 = 0.1$  meV. This figure corresponds to numerical parameters closer to that of molecules. For this case, we observe that the two spectra start to differ for  $\hbar\gamma \lesssim 0.2 - 0.4$  meV, and the condition in Eq. (21) gives  $\hbar\gamma \lesssim 0.25$  meV, which is challenging to achieve experimentally but within reach [56]. Finally, we apply the criterion in Eq. (21) to the results in Fig. 4(b). In this case,  $\hbar\Omega_0 = \hbar\gamma = 1$  meV, which gives the threshold  $\sigma_L/a \lesssim 2\pi$  when the dipole-dipole interactions need to be explicitly considered, in good agreement with the numerical results.

## V. CONCLUSION

We have studied the effect of direct molecular dipole-dipole interactions on the optical response of photonic nanocavities strongly coupled with molecular assemblies or 2D materials. The description was based on a CQED approach to the dynamics of the states in the system, without rotating-wave approximation and including the losses via an effective broadening of the modes. An alternative approach to model the system based on classical dipoles or coupled harmonic oscillators is also possible.

As a first step, we described how, in the absence of the nanocavity, the dipole-dipole interactions lead to the emergence of collective modes that span a significant frequency range and are characterized by a very large wave vector in the in-plane direction. It was thus possible to obtain a dispersion relation and we found that it resembles the one characterizing an infinite layer, even for a relatively small molecular patch with a lateral size of only  $N \times a \approx 25$  nm (to be compared with the much larger wavelength).

When the photonic nanocavity was included, the influence of the direct molecule-molecule interactions on the optical response of the coupled system strongly depended on the degree of localization of the cavity fields. For homogeneous or slowly varying fields, the effect of these interactions was mostly a direct renormalization of the vibrational resonant frequency. However, when the fields were confined to the level of a few intermolecular distances, conditions existed under which direct interactions could show a more profound effect. Instead of observing the two clear polaritonic peaks, as occurs for no direct interactions, one of the polaritonic modes could spread out into many (weaker) subpeaks. We attributed this observation to the fact that, as a consequence of the direct molecule-molecule interaction, multiple collective modes at different frequencies and wave vectors could couple (less efficiently) with the photonic nanocavity and contribute to the response.

We further derived a simple equation that indicated the conditions for this effect of dipole-dipole interaction to become relevant, beyond the energy renormalization. In general, molecules (or 2D materials) characterized by strong transition dipole moment and/or weak losses were required, together with large field localization. Several 2D materials are characterized by low losses and large vibrational dipole moments, which could reach the dipole-dipole coupling strength  $\hbar\Omega_0 \approx 1$  meV used in most of our calculations (Appendix A). Molecules are generally characterized by weaker  $\Omega_0$ , but their associated losses could also be sufficiently small. For example, several vibrations of the molecule 4, 4'-bis(*N*-carbazolyl)-1, 1'-biphenyl (CBP) have losses of  $\gamma_{\text{mol}} \approx 0.7 - 1.74$  meV  $\approx (0.04 - 0.1)\omega_{\text{mol}}$  and the losses of h-BN lattice vibrations (phonons) are  $\gamma_{\text{h-BN}} \approx 0.5 - 0.6$  meV [56]. Further, the vibrational losses for a single molecule embedded in a matrix can be as small as 0.07 meV (10-ps lifetime).

Our results thus identify the conditions where it becomes necessary to include explicitly direct molecule-molecule interactions to describe the optical response of a coupled system beyond a renormalization of the energy. Furthermore, we have focused our study on the coupling with molecular vibrations

or phonons, but the analysis and conclusions can be applied to other transitions (such as molecular excitonic transitions) in a straightforward manner. For example, it is interesting to consider the coupling of plasmonic systems with excitonic transitions characterized by large dipole moment and present in quantum emitters such as molecules or quantum dots. The coupling strength can be very large in these systems [57–59], and the losses of the excitonic transitions are only limited by the spontaneous decay rate and can thus in principle be extremely small at cryogenic temperature. On the other hand, plasmonic losses and room-temperature excitonic losses can be large, so it is important to consider the details of each experimental configuration.

#### ACKNOWLEDGMENTS

We would like to acknowledge Unai Muniain for fruitful discussions. This work was supported by Grant No. PID2019-107432GB-I00 funded by MCIN/AEI/10.13039/501100011033 and Grant No. IT 1526-22 from the Basque Government for consolidated groups of the Basque University, as well as the European Union (NextGenerationEU) through the Complementary Plans (Grant No. PRTR-C17.I1) promoted by the Ministry of Science and Innovation within the Recovery, Transformation, and Resilience Plan of Spain, and part of the activities of the IKUR strategy of the Department of Education promoted by the Basque Government.

#### APPENDIX A: ESTIMATION OF $\Omega_0$ FOR REAL MATERIALS

To estimate the value of  $\Omega_0$ , we consider first a simple description of the relative permittivity  $\varepsilon_r$  of a polar material at a frequency  $\omega$ , near a phonon resonance. Ignoring losses, we obtain

$$\varepsilon_r(\omega) = \varepsilon_\infty \left( 1 + \frac{\omega_L^2 - \omega_T^2}{\omega_T^2 - \omega^2} \right), \quad (\text{A1})$$

where  $\omega_L$  and  $\omega_T$  are the longitudinal and transverse phonon frequencies, respectively, and  $\varepsilon_\infty$  is the high-frequency permittivity. This permittivity corresponds to a transition dipole moment  $d_u$  per unit cell of volume  $V_{\text{cell}}$  [26],

$$d_u = \sqrt{\frac{\hbar}{2\omega_T}} V_{\text{cell}} \varepsilon_0 \varepsilon_\infty (\omega_L^2 - \omega_T^2), \quad (\text{A2})$$

where  $\varepsilon_0$  is the vacuum permittivity. Assuming, for simplicity, a cubic structure  $V_{\text{cell}} = a^3$ , with  $a$  the lattice parameter of the unit cell, we obtain

$$\Omega_0 = \frac{|d_u|^2}{4\pi \varepsilon_0 \varepsilon_\infty \hbar a^3} = \frac{\omega_L^2 - \omega_T^2}{8\pi \omega_T}. \quad (\text{A3})$$

For this derivation we have considered an arbitrary value of  $\varepsilon_\infty$  to show that it does not affect the final result. The model in the main text corresponds to  $\varepsilon_\infty = 1$  as only one vibrational mode is included.

As an example, we obtain  $\Omega_0 = 0.0196\omega_T$  for SiC [60] and  $\Omega_0 = 0.016\omega_T$  and  $0.008\omega_T$  for the in-plane and out-of-plane modes of h-BN, respectively [26]. These values are comparable to the value  $\Omega_0 = 0.01\omega_{\text{mol}}$  used in the main text, although

a more rigorous model would need to consider that the unit cell of these materials is not cubic, that we are comparing here with a bulk material and not a monolayer, and that  $\omega_{\text{mol}}$  does not exactly correspond to  $\omega_L$  or  $\omega_T$ .

We can also proceed in the same manner for molecular ensembles. We note that the permittivity is in this case typically written in a different form, such as

$$\varepsilon_r(\omega) = \varepsilon_\infty + \frac{S^2}{\omega_{\text{mol}}^2 - \omega^2}, \quad (\text{A4})$$

where  $S$  sets the strength of the resonance and  $\omega_{\text{mol}}$  is the resonant frequency. Proceeding in the same way as before, we obtain

$$\Omega_0 = \frac{S^2}{8\pi \omega_{\text{mol}} \varepsilon_\infty}. \quad (\text{A5})$$

For CBP [30],  $\varepsilon_\infty = 2.8$  and the vibrational peak at  $\omega_{\text{mol}} = 1504 \text{ cm}^{-1}$  is characterized by  $S = 164 \text{ cm}^{-1}$ , which gives  $\Omega_0 = 1.7 \times 10^{-4} \omega_{\text{mol}}$ .

#### APPENDIX B: OPTICAL RESPONSE OF THE VIBRATIONAL MODES WITH LATTICE CONSTANT $a$

The lattice constant will change the results of our discussion in the main text quantitatively, but not qualitatively. For homogeneous fields, changing the lattice constant would have the same effect as changing the coupling strength  $\Omega_0 \propto 1/a^3$ , which we explore in Fig. 3(b). For inhomogeneous fields, i.e., confined fields, changing  $a$  can involve several effects simultaneously (change of  $\Omega_0$ , change of the normalized confinement  $\sigma_L/a$ , and change of the coupling strength  $g_j$ ).

Here we explore two different situations where we change the lattice constant  $a$ . In Fig. 7(a) we show the case where we fix  $g_j$  and  $g_{\text{tot}}$  and in Fig. 7(b) the case where we fix  $g_{\text{tot}}$  and  $\sigma_L$ . We show the results for a nanophotonic cavity which couples with the 2D molecular square patch containing  $N = 51 \times 51 = 2601$  molecules as a function of the lattice constant  $a$ , considering  $\hbar\Omega_0 = 0.125/a^3 \text{ meV}$ . We set for each case  $\omega_{\text{cav}} = W_1$  and  $\hbar g_{\text{tot}} = 2 \text{ meV}$ .

#### APPENDIX C: THEORETICAL DISPERSION RELATION OF AN INFINITE MONOLAYER

In the main text we numerically solved for the collective excitations of the finite system arising from the direct dipole-dipole interactions. On the other hand, it is possible to obtain the analytical dispersion relation of the infinite 2D molecular monolayer by taking a solid-state approach, where quasiexcitations propagate on a lattice. Each molecule is indexed by  $s$  and is located at  $\mathbf{r}_s$ . The total vibronic Hamiltonian becomes

$$\begin{aligned} \hat{H}_{\text{mol}} + \hat{H}_{\text{vib-vib}} &= \hbar \sum_s \omega_{\text{mol}} \hat{b}_s^\dagger \hat{b}_s \\ &+ \hbar \sum_s \sum_{s' > s} \Omega_{|\mathbf{r}_{s'} - \mathbf{r}_s|} (\hat{b}_s^\dagger + \hat{b}_s) (\hat{b}_{s'}^\dagger + \hat{b}_{s'}). \end{aligned} \quad (\text{C1})$$

The equations of motion for the expectation values  $\beta_s = \langle \hat{b}_s \rangle$  can be obtained from  $d\hat{b}_s/dt = -i/\hbar [\hat{b}_s, \hat{H}_{\text{mol}} + \hat{H}_{\text{vib-vib}}]$ . To better illustrate the procedure to obtain the dispersion relation,

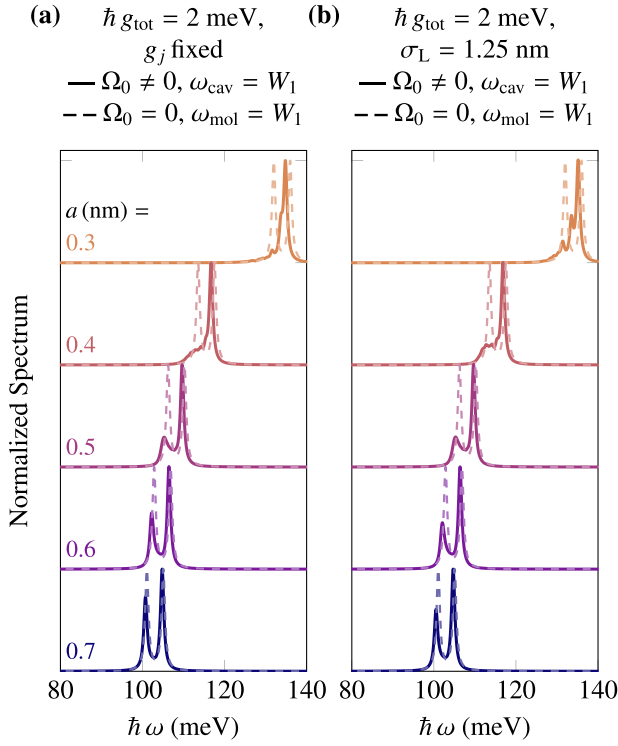


FIG. 7. Influence of the direct dipole-dipole interactions on the optical spectrum  $S(\omega)$  for different values of the lattice constant  $a$ . The normalized optical spectrum of an IR cavity coupled to a 2D square lattice with  $N = 51 \times 51 = 2601$  molecules is plotted, keeping the total coupling fixed at  $\hbar g_{\text{tot}} = 2$  meV and including (solid lines) or ignoring (dashed lines) direct molecule-molecule interactions. The former considers vibrational energy  $\hbar\omega_{\text{mol}} = 100$  meV and the latter  $\omega_{\text{mol}} = W_1$ . (a) Each equivalent molecule (in the same lattice position  $j$ ) experiences the same coupling strength  $g_j$ , which requires changing  $\sigma_L$  appropriately (for reference, when  $a = 0.5$  nm,  $\sigma_L = 2.5a$ ). (b) Same as in (a) but the field distribution  $\sigma_L = 1.25$  nm is kept fixed. The spectra are shifted vertically for visibility and are obtained for  $\hbar\gamma = 1$  meV, and  $\hbar\Omega_0 = 0.125/a^3$  meV. In all the spectra, the value of the resonant cavity frequency  $\omega_{\text{cav}}$  is set equal to the corresponding value of  $W_1$ .

we first consider a 1D chain, assume nearest-neighbor coupling  $\Omega_{|\mathbf{r}_s - \mathbf{r}_s|} = \Omega_{j,j\pm 1} \equiv \Omega_0$  and neglect the terms  $\hat{b}_s \hat{b}_s'$  and  $\hat{b}_s^\dagger \hat{b}_s'^\dagger$  that describe the creation and annihilation of two vibrations at the same time [rotating-wave approximation (RWA)]. By doing so, we arrive at

$$\dot{\beta}_j = -i\omega_{\text{mol}}\beta_j - i\Omega_0(\beta_{j-1} + \beta_{j+1}).$$

We then insert the ansatz  $\beta_j = \mathcal{B}_k e^{i(kaj - \omega t)}$  into the above equation, where  $a$  is the lattice constant, and obtain

$$\omega = \omega_{\text{mol}} + \Omega_0(e^{ika} + e^{-ika}), \quad (\text{C2})$$

which straightforwardly leads to the dispersion relation

$$\omega = \omega_{\text{mol}} + 2\Omega_0 \cos(ka). \quad (\text{C3})$$

This result has the advantage of simplicity, but does not show the right tendency for low values of  $\mathbf{k}$ , where the coupling with a significant number of neighbors beyond the nearest one can contribute to the result. However, the

procedure described can be extended to all neighbors in a straightforward manner. The equations of motions are in this case  $\dot{\beta}_j = -i\omega_{\text{mol}}\beta_j - i \sum_{l \neq j} \Omega_{jl} \beta_l$ . Using the ansatz  $\beta_j = \mathcal{B}_k e^{i(\mathbf{k} \cdot \mathbf{r}_j - \omega t)}$  with  $\mathbf{r}_{lj} = \mathbf{r}_l - \mathbf{r}_j$  gives the dispersion relation

$$\omega = \omega_0 + \sum_{l \neq j} \frac{\Omega_{lj}}{2} (e^{i\mathbf{k} \cdot \mathbf{r}_{lj}} + e^{-i\mathbf{k} \cdot \mathbf{r}_{lj}}), \quad (\text{C4})$$

with the factor of  $\frac{1}{2}$  to avoid double counting and  $\Omega_{lj}$  as defined in Eq. (3), where the sum runs over all  $l \neq j$ , with  $j$  an arbitrary number

### 1. Dispersion relation beyond the RWA

For the relatively small values of  $\Omega_0$  used in the main text, the RWA [used to derive Eq. (C4)] is a good approximation. However, for completeness, we derive next the dispersion relation without the RWA, i.e., including the terms that do not conserve the number of excitations. We begin by considering again only coupling between nearest neighbors in a 1D chain. The equations of motion become

$$\begin{aligned} \dot{\beta}_j &= -i\omega_{\text{mol}}\beta_j - i\Omega_0\beta_{j-1} - i\Omega_0\beta_{j+1} - i\Omega_0\beta_{j-1}^* - i\Omega_0\beta_{j+1}^*, \\ \dot{\beta}_j^* &= i\omega_{\text{mol}}\beta_j^* + i\Omega_0\beta_{j-1}^* + i\Omega_0\beta_{j+1}^* + i\Omega_0\beta_{j-1} + i\Omega_0\beta_{j+1}. \end{aligned}$$

Defining  $A_j = \beta_j + \beta_j^*$  and  $B_j = \beta_j - \beta_j^*$ , we get

$$\begin{aligned} \frac{d}{dt} A_j &= -i\omega_{\text{mol}} B_j, \\ \frac{d}{dt} B_j &= -i\omega_{\text{mol}} A_j - i2\Omega_0(A_{j-1} + A_{j+1}). \end{aligned}$$

Taking the time derivative of the first equation, we find

$$\frac{d^2}{dt^2} A_j = -\omega_{\text{mol}}^2 A_j - 2\omega_{\text{mol}} \Omega_0 (A_{j-1} + A_{j+1}).$$

Following the same procedure as before, with the ansatz  $A_j = e^{i(kaj - \omega t)}$ , results in

$$\omega = \sqrt{\omega_{\text{mol}}^2 + 2\omega_{\text{mol}} \Omega_0 (e^{ika} + e^{-ika})}. \quad (\text{C5})$$

On the other hand, if we proceed in the same manner but expand to all possible neighbors, we obtain the final dispersion relation

$$\omega = \sqrt{\omega_{\text{mol}}^2 + \omega_{\text{mol}} \sum_{l \neq j} \Omega_{lj} (e^{i\mathbf{k} \cdot \mathbf{r}_{lj}} + e^{-i\mathbf{k} \cdot \mathbf{r}_{lj}})}, \quad (\text{C6})$$

with a factor  $\frac{1}{2}$  again included when we expand to more molecules. Equation (C6) reduces to the RWA in the limit of small  $\Omega_{lj}$ , as expected.

In Fig. 8 we compare the numerical dispersion relation for a finite ( $N = 51 \times 51$ ) number of molecules (without nanocavity), obtained as in Fig. 2(e), with the analytical dispersion of the infinite monolayer. The latter is evaluated in the range  $k_{x,y} = [0, \pi/a]$  with increments of  $\pi/100a$ . The results for  $\hbar\Omega_0 = 0.8$  meV in Fig. 8(a) show good agreement between the numerical results of the finite system (blue squares) and the analytical results of the infinite monolayer within the RWA [Eq. (C4), lilac circles]. The exact theoretical dispersion of the infinite monolayer obtained without the RWA [Eq. (C6)]

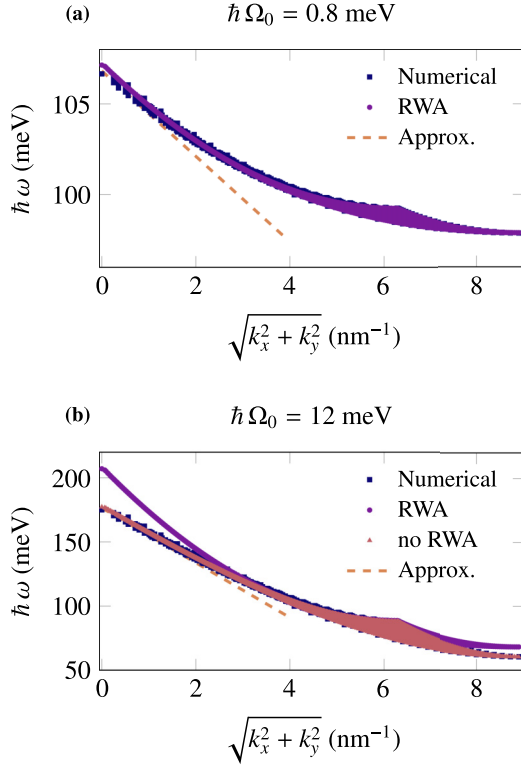


FIG. 8. Dispersion relation for dipole-dipole interaction strength between the molecules: (a)  $\hbar\Omega_0 = 0.8$  meV and (b)  $\hbar\Omega_0 = 12$  meV. The molecules are placed in a square lattice with lattice constant  $a = 0.5$  nm and  $\hbar\omega_{\text{mol}} = 100$  meV. We compare the numerical results of the eigenvalues  $W_n$  for  $N = 51 \times 51 = 2601$  molecules (blue squares) with the analytical expression for an infinite monolayer obtained with [lilac circles, Eq. (C4)] and without [pink triangles, Eq. (C6)] the RWA. The analytical equations are evaluated for a range of  $k_{x,y} = [0, \pi/a]$ . Dashed lines show the linear approximation according to Eq. (C7).

is not shown, but it is almost identical to that obtained with the RWA.

To illustrate a situation that requires going beyond the RWA, we plot in Fig. 8(b) the dispersion relation for a very large  $\hbar\Omega_0 = 12$  meV. This large coupling leads to a significantly larger span of energies of the collective modes. We find again that the exact theoretical dispersion of the infinite system, as obtained without the RWA (orange triangles) [Eq. (C6)], matches well the numerical results for the finite number of molecules (blue squares). However, the theoretical dispersion of the infinite system obtained within the RWA (lilac circles) [Eq. (C4)] is markedly different from both.

Figure 8 also shows a spreading of the data points in the dispersion relation. To explain its origin, we plot in Fig. 9(a) the Brillouin zone for a lattice with a square unit cell, where we enhance the triangle formed by the critical points  $\Gamma$ ,  $X$ , and  $M$ . The dispersion is shown schematically in Fig. 9(b). For each wave vector  $|\mathbf{k}| = \sqrt{k_x^2 + k_y^2}$ , the eigenvalues extend over a range of energies. The eigenvectors with wave vector pointing in the direction  $\Gamma$ - $X$  of the Brillouin zone ( $k_y = 0$ , maximum value  $k_x^{\text{max}} = \pi/a$ ) correspond to the points of largest energy for each  $|\mathbf{k}|$ . Similarly, eigenvectors with wave

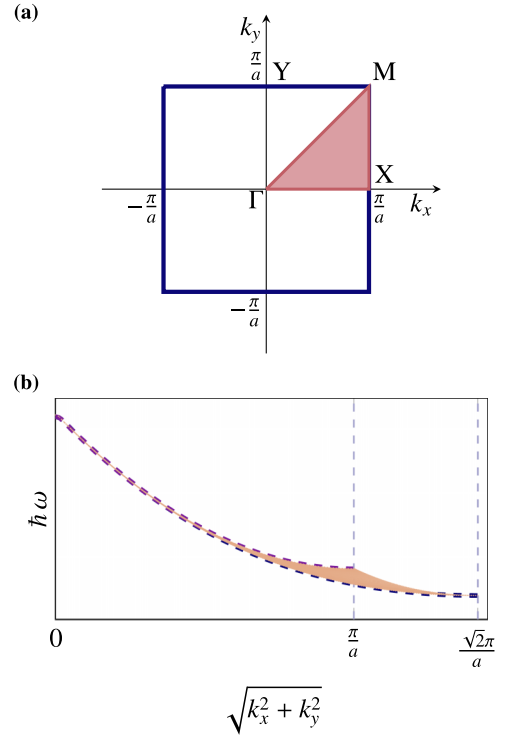


FIG. 9. (a) Brillouin zone of the square lattice. The critical points (points of high symmetry)  $\Gamma$ ,  $M$ ,  $X$ , and  $Y$  are depicted. (b) Illustrative example of a typical dispersion relation for a square lattice with dipole-dipole interactions (shaded orange area). For a fixed  $\sqrt{k_x^2 + k_y^2}$ , the energies of the collective vibrational modes show a certain spread so that they are contained within the two dashed blue lines shown in the plot. The upper blue dashed line corresponds to wave vectors in the  $\Gamma$ - $X$  direction in the reciprocal space, with  $k_y = 0$  and  $k_x \leq \pi/a$ . The lower blue dashed line corresponds to wave vectors in the  $\Gamma$ - $M$  direction [ $k_x = k_y$  and  $\sqrt{(k_x^{\text{max}})^2 + (k_y^{\text{max}})^2} = \sqrt{2}(\pi/a)$ ].

vector in the  $\Gamma$ - $M$  direction ( $k_x = k_y$ ), with maximum value  $\sqrt{(k_x^{\text{max}})^2 + (k_y^{\text{max}})^2} = \sqrt{2}(\pi/a)$ , results in the lowest-energy solutions. The eigenenergies corresponding to these two directions are highlighted in the figure by the blue dashed lines.

## 2. Linear approximation for $\mathbf{k} \rightarrow 0$

The dispersion relations in Fig. 8 show a linear dependence between the energy and the modulus  $|\mathbf{k}|$  of the wave vector for small  $\mathbf{k}$ . For simplicity, we consider the case  $k_y = 0$ , as the results show the same slope with  $|\mathbf{k}| = \sqrt{k_x^2 + k_y^2}$ , independently of the individual weights of  $k_x$  and  $k_y$ . Moreover, since we are considering a square lattice with constant  $a$ , let us write the positions  $x_l = am$  and  $y_j = an$ . In this case, Eq. (C6) becomes

$$\omega = \sqrt{\omega_{\text{mol}}^2 + 2\omega_{\text{mol}}\Omega_0 \sum_{m,n} \frac{\cos(k_x am)}{(\sqrt{m^2 + n^2})^3}},$$

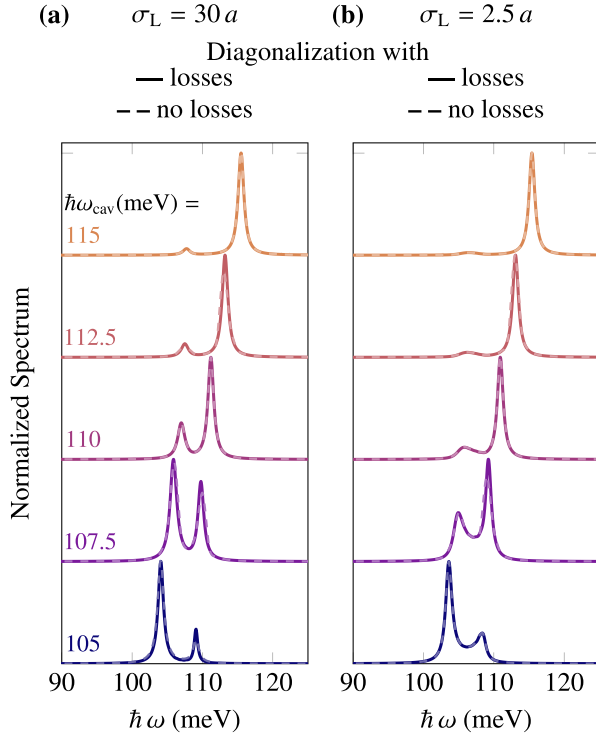


FIG. 10. Comparison of the results obtained using two different procedures to incorporate losses in the spectral response. Normalized spectra are shown for a 2D lattice with  $N = 51 \times 51 = 2601$  molecules with lattice constant 0.5 nm and  $\hbar\omega_{\text{mol}} = 100$  meV that couple with an IR cavity mode characterized by field confinement (a)  $\sigma_L = 30a$  and (b)  $\sigma_L = 2.5a$ . In both cases,  $\hbar g_{\text{tot}} = \hbar\sqrt{\sum_j |g_j(\mathbf{r})|^2} = 2$  meV and the dipole-dipole coupling strength is  $\hbar\Omega_0 = 1$  meV ( $\hbar W_1 \approx 108.2$  meV). The solid lines correspond to the results obtained when incorporating molecular,  $\hbar\Gamma = 1$  meV, and plasmonic losses,  $\hbar\kappa = 1$  meV, directly in the Hamiltonian and applying Eq. (D1). The dashed lines are obtained, as in the main text, by solving the Hamiltonian without losses and then applying Eq. (18) with line broadening  $\hbar\gamma = 1$  meV. The spectra are shifted vertically for visibility.

where the sum runs from  $m, n = -N/2$  to  $N/2$ , excluding  $n = m$ . At  $k_x = 0$ , this expression takes the value

$$\omega(k_x = 0) = \sqrt{\omega_{\text{mol}}^2 + 2\omega_{\text{mol}} \sum_{m,n} \frac{\Omega_0}{(\sqrt{m^2 + n^2})^3}}.$$

To find the slope, we first focus on the term

$$2\omega_{\text{mol}}\Omega_0 \sum_{m,n} \frac{\cos(k_x am)}{(\sqrt{m^2 + n^2})^3}$$

inside the square root. The derivative of this term with respect to  $k_x$  is

$$-2\omega_{\text{mol}}\Omega_0 \sum_{m,n} \frac{am \sin(k_x am)}{(\sqrt{m^2 + n^2})^3}.$$

Interestingly, all the individual terms are null at  $k_x = 0$ , but the infinite sum is not, which indicates that the value of the sum

at  $k_x = 0$  is determined by the terms corresponding to large  $m^2 + n^2$ . Based on this, we convert the sum in  $m$  and  $n$  to an integral, which can be solved analytically:

$$-2\omega_{\text{mol}}\Omega_0 \int_{-\infty}^{\infty} dx \int_{-\infty}^{\infty} dy \frac{ax \sin(k_x ax)}{(\sqrt{x^2 + y^2})^3} = -4\pi\omega_{\text{mol}}\Omega_0 a.$$

The energies at low values of  $k_x$  thus follow

$$\omega = \sqrt{\omega_{\text{mol}}^2 + 2\omega_{\text{mol}} \sum_{m,n} \frac{\Omega_0}{(\sqrt{m^2 + n^2})^3} - 4\pi\omega_{\text{mol}}\Omega_0 a k_x}.$$

Expanding this expression to first order and substituting  $k_x \rightarrow |\mathbf{k}| = \sqrt{k_x^2 + k_y^2}$  (discussed above), we obtain

$$\omega = \sqrt{\omega_{\text{mol}}^2 + 2\omega_{\text{mol}} \sum_{m,n} \frac{\Omega_0}{(\sqrt{m^2 + n^2})^3}} - \frac{2\pi\Omega_0 |\mathbf{k}| a \omega_{\text{mol}}}{\sqrt{\omega_{\text{mol}}^2 + 2\omega_{\text{mol}} \sum_{m,n} \frac{\Omega_0}{(\sqrt{m^2 + n^2})^3}}}. \quad (\text{C7})$$

For  $\Omega_0 \ll \omega_{\text{mol}}$  the second term of the denominator can be ignored and Eq. (C7) becomes Eq. (20). The dispersion given by Eq. (C7) is also plotted in Fig. 8 (dashed line) and shows good agreement with the numerical results for low  $|\mathbf{k}|$ .

#### APPENDIX D: COMPARING DIFFERENT WAYS OF INCLUDING LOSSES

We incorporated the losses in the spectra of the main text by changing the  $\delta$  functions obtained in the spectral function when no losses are considered into Lorentzian lines of full width at half maximum  $\gamma$ . In the following, we compare these results to those obtained by performing the transformation  $\omega_{\text{cav}} \rightarrow \omega_{\text{cav}} + i\kappa/2$  and  $\omega_{\text{mol}} \rightarrow \omega_{\text{mol}} + i\Gamma/2$  and numerically diagonalizing the full Hamiltonian of the system to find the new eigenvalues. For simplicity, we consider molecular losses  $\hbar\Gamma = 1$  meV and different cavities with  $\hbar\kappa = 1$  meV. As the new eigenvectors of the system  $\mathcal{W}_m$  are no longer real, we use the same definition as in Eq. (18) but modified as

$$S(\omega) = \sum_m (|\zeta_{m1}|^2 - |\eta_{m1}|^2) \times \frac{\text{Im}(\mathcal{W}_m)}{[\omega - \text{Re}(\mathcal{W}_m)]^2 + [\text{Im}(\mathcal{W}_m)]^2}, \quad (\text{D1})$$

in order to compare both results.

In Fig. 10 we compare the results obtained in the main text [Eq. (18), dashed lines] with those obtained using the procedure described in this Appendix (solid lines). The results are obtained for the same system as in Fig. 1(a) ( $N = 51 \times 51$  dipoles in a monolayer coupled to a cavity mode), for small  $\sigma_L = 30a$  [Fig. 10(a)] and large  $\sigma_L = 2.5a$  [Fig. 10(b)] localization of the cavity fields. The results are very similar in both of the procedures used to incorporate losses.

- [1] V. M. Agranovich, M. Litinskaia, and D. G. Lidzey, Cavity polaritons in microcavities containing disordered organic semiconductors, *Phys. Rev. B* **67**, 085311 (2003).
- [2] J. P. Long and B. S. Simpkins, Coherent coupling between a molecular vibration and Fabry-Perot optical cavity to give hybridized states in the strong coupling limit, *ACS Photon.* **2**, 130 (2015).
- [3] A. Shalabney, J. George, J. Hutchison, G. Pupillo, C. Genet, and T. W. Ebbesen, Coherent coupling of molecular resonators with a microcavity mode, *Nat. Commun.* **6**, 5981 (2015).
- [4] J. George, A. Shalabney, J. A. Hutchison, C. Genet, and T. W. Ebbesen, Liquid-phase vibrational strong coupling, *J. Phys. Chem. Lett.* **6**, 1027 (2015).
- [5] B. S. Simpkins, K. P. Fears, W. J. Dressick, B. T. Spann, A. D. Dunkelberger, and J. C. Owrutsky, Spanning strong to weak normal mode coupling between vibrational and Fabry-Pérot cavity modes through tuning of vibrational absorption strength, *ACS Photon.* **2**, 1460 (2015).
- [6] J. Lather, P. Bhatt, A. Thomas, T. W. Ebbesen, and J. George, Cavity catalysis by cooperative vibrational strong coupling of reactant and solvent molecules, *Angew. Chem.* **58**, 10635 (2019).
- [7] D. G. Lidzey, D. D. C. Bradley, M. S. Skolnick, T. Virgili, S. Walker, and D. M. Whittaker, Strong exciton-photon coupling in an organic semiconductor microcavity, *Nature (London)* **395**, 53 (1998).
- [8] D. G. Lidzey, D. D. C. Bradley, T. Virgili, A. Armitage, M. S. Skolnick, and S. Walker, Room temperature polariton emission from strongly coupled organic semiconductor microcavities, *Phys. Rev. Lett.* **82**, 3316 (1999).
- [9] D. G. Lidzey, D. D. C. Bradley, A. Armitage, S. Walker, and M. S. Skolnick, Photon-mediated hybridization of Frenkel excitons in organic semiconductor microcavities, *Science* **288**, 1620 (2000).
- [10] H. Leng, B. Szychowski, M.-C. Daniel, and M. Pelton, Strong coupling and induced transparency at room temperature with single quantum dots and gap plasmons, *Nat. Commun.* **9**, 4012 (2018).
- [11] J. Schachenmayer, C. Genes, E. Tignone, and G. Pupillo, Cavity-enhanced transport of excitons, *Phys. Rev. Lett.* **114**, 196403 (2015).
- [12] D. Melnikau, R. Esteban, D. Savateeva, A. Sánchez-Iglesias, M. Grzelczak, M. K. Schmidt, L. M. Liz-Marzán, J. Aizpurua, and Y. P. Rakovich, Rabi splitting in photoluminescence spectra of hybrid systems of gold nanorods and J-aggregates, *J. Phys. Chem. Lett.* **7**, 354 (2016).
- [13] F. Wu, J. Guo, Y. Huang, K. Liang, L. Jin, J. Li, X. Deng, R. Jiao, Y. Liu, J. Zhang, W. Zhang, and L. Yu, Plexcitonic optical chirality: Strong exciton-plasmon coupling in chiral J-aggregate-metal nanoparticle complexes, *ACS Nano* **15**, 2292 (2021).
- [14] J. Feist, J. Galego, and F. J. Garcia-Vidal, Polaritonic chemistry with organic molecules, *ACS Photon.* **5**, 205 (2018).
- [15] J. Flick, M. Ruggenthaler, H. Appel, and A. Rubio, Atoms and molecules in cavities, from weak to strong coupling in quantum-electrodynamics (QED) chemistry, *Proc. Natl. Acad. Sci. USA* **114**, 3026 (2017).
- [16] F. Herrera and F. C. Spano, Cavity-controlled chemistry in molecular ensembles, *Phys. Rev. Lett.* **116**, 238301 (2016).
- [17] R. M. A. Vergauwe, A. Thomas, K. Nagarajan, A. Shalabney, J. George, T. Chervy, M. Seidel, E. Devaux, V. Torbeev, and T. W. Ebbesen, Modification of enzyme activity by vibrational strong coupling of water, *Angew. Chem. Int. Ed.* **58**, 15324 (2019).
- [18] A. Thomas, L. Lethuillier-Karl, K. Nagarajan, R. M. A. Vergauwe, J. George, T. Chervy, A. Shalabney, E. Devaux, C. Genet, J. Moran, and T. W. Ebbesen, Tilting a ground-state reactivity landscape by vibrational strong coupling, *Science* **363**, 615 (2019).
- [19] J. Galego, F. J. Garcia-Vidal, and J. Feist, Cavity-induced modifications of molecular structure in the strong-coupling regime, *Phys. Rev. X* **5**, 041022 (2015).
- [20] S. M. Dutra, *Cavity Quantum Electrodynamics* (Wiley, New York, 2004).
- [21] P. Törmä and W. L. Barnes, Strong coupling between surface plasmon polaritons and emitters: A review, *Rep. Prog. Phys.* **78**, 013901 (2014).
- [22] T. W. Ebbesen, Hybrid light-matter states in a molecular and material science perspective, *Accounts Chem. Res.* **49**, 2403 (2016).
- [23] B. Xiang and W. Xiong, Molecular vibrational polariton: Its dynamics and potentials in novel chemistry and quantum technology, *J. Chem. Phys.* **155**, 050901 (2021).
- [24] B. Xiang, R. F. Ribeiro, A. D. Dunkelberger, J. Wang, Y. Li, B. S. Simpkins, J. C. Owrutsky, J. Yuen-Zhou, and W. Xiong, Two-dimensional infrared spectroscopy of vibrational polaritons, *Proc. Natl. Acad. Sci. USA* **115**, 4845 (2018).
- [25] H. Benisty, J.-J. Greffet, and P. Lalanne, *Introduction to Nanophotonics* (Oxford University Press, Oxford, 2022).
- [26] M. Barra-Burillo, U. Muniain, S. Catalano, M. Autore, F. Casanova, L. E. Hueso, J. Aizpurua, R. Esteban, and R. Hillenbrand, Microcavity phonon polaritons from the weak to the ultrastrong phonon-photon coupling regime, *Nat. Commun.* **12**, 6206 (2021).
- [27] N. J. Schilder, C. Sauvan, J.-P. Hugonin, S. Jennewein, Y. R. P. Sortais, A. Browaeys, and J.-J. Greffet, Polaritonic modes in a dense cloud of cold atoms, *Phys. Rev. A* **93**, 063835 (2016).
- [28] S. Jennewein, M. Besbes, N. J. Schilder, S. D. Jenkins, C. Sauvan, J. Ruostekoski, J.-J. Greffet, Y. R. P. Sortais, and A. Browaeys, Coherent scattering of near-resonant light by a dense microscopic cold atomic cloud, *Phys. Rev. Lett.* **116**, 233601 (2016).
- [29] D. N. Basov, M. M. Fogler, and F. J. G. de Abajo, Polaritons in van der Waals materials, *Science* **354**, aag1992 (2016).
- [30] M. Autore, P. Li, I. Dolado, F. J. Alfaro-Mozaz, R. Esteban, A. Atxabal, F. Casanova, L. E. Hueso, P. Alonso-González, J. Aizpurua, A. Y. Nikitin, S. Vélez, and R. Hillenbrand, Boron nitride nanoresonators for phonon-enhanced molecular vibrational spectroscopy at the strong coupling limit, *Light Sci. Appl.* **7**, 17172 (2018).
- [31] W. Ma, P. Alonso-González, S. Li, A. Y. Nikitin, J. Yuan, J. Martín-Sánchez, J. Taboada-Gutiérrez, I. Amenabar, P. Li, S. Vélez, C. Tollan, Z. Dai, Y. Zhang, S. Sriram, K. Kalantar-Zadeh, S.-T. Lee, R. Hillenbrand, and Q. Bao, In-plane anisotropic and ultra-low-loss polaritons in a natural van der Waals crystal, *Nature (London)* **562**, 557 (2018).
- [32] D. A. Iranzo, S. Nanot, E. J. C. Dias, I. Epstein, C. Peng, D. K. Efetov, M. B. Lundberg, R. Parret, J. Osmond, J.-Y. Hong, J. Kong, D. R. Englund, N. M. R. Peres, and F. H. L. Koppens,

- Probing the ultimate plasmon confinement limits with a van der Waals heterostructure, *Science* **360**, 291 (2018).
- [33] M. Singh, N. Kaur, and E. Comini, The role of self-assembled monolayers in electronic devices, *J. Mater. Chem. C* **8**, 3938 (2020).
- [34] R. Zhang, Y. Zhang, Z. C. Dong, S. Jiang, C. Zhang, L. G. Chen, L. Zhang, Y. Liao, J. Aizpurua, Y. Luo, J. L. Yang, and J. G. Hou, Chemical mapping of a single molecule by plasmon-enhanced Raman scattering, *Nature (London)* **498**, 82 (2013).
- [35] M. Barbry, P. Koval, F. Marchesin, R. Esteban, A. G. Borisov, J. Aizpurua, and D. Sánchez-Portal, Atomistic near-field nanoplasmonics: Reaching atomic-scale resolution in nanooptics, *Nano Lett.* **15**, 3410 (2015).
- [36] F. Benz, M. K. Schmidt, A. Dreismann, R. Chikkaraddy, Y. Zhang, A. Demetriadou, C. Carnegie, H. Ohadi, B. de Nijs, R. Esteban, J. Aizpurua, and J. J. Baumberg, Single-molecule optomechanics in picocavities, *Science* **354**, 726 (2016).
- [37] B. Doppagne, M. C. Chong, H. Bulou, A. Boeglin, F. Scheurer, and G. Schull, Electrofluorochromism at the single-molecule level, *Science* **361**, 251 (2018).
- [38] L. A. Jakob, W. M. Deacon, Y. Zhang, B. de Nijs, E. Pavlenko, S. Hu, C. Carnegie, T. Neuman, R. Esteban, J. Aizpurua, and J. J. Baumberg, Giant optomechanical spring effect in plasmonic nano- and picocavities probed by surface-enhanced Raman scattering, *Nat. Commun.* **14**, 3291 (2023).
- [39] B. Doppagne, M. C. Chong, E. Lorchat, S. Berciaud, M. Romeo, H. Bulou, A. Boeglin, F. Scheurer, and G. Schull, Vibronic spectroscopy with submolecular resolution from STM-induced electroluminescence, *Phys. Rev. Lett.* **118**, 127401 (2017).
- [40] A. Frisk Kockum, A. Miranowicz, S. De Liberato, S. Savasta, and F. Nori, Ultrastrong coupling between light and matter, *Nat. Rev. Phys.* **1**, 19 (2019).
- [41] T. Tufarelli, K. R. McEnery, S. A. Maier, and M. S. Kim, Signatures of the  $A^2$  term in ultrastrongly coupled oscillators, *Phys. Rev. A* **91**, 063840 (2015).
- [42] N. N. Bogoljubov, On a new method in the theory of superconductivity, *Nuovo Cimento* **7**, 794 (1958).
- [43] J. J. Hopfield, Theory of the contribution of excitons to the complex dielectric constant of crystals, *Phys. Rev.* **112**, 1555 (1958).
- [44] Y. Todorov, L. Toso, A. Delteil, A. Vasanelli, C. Sirtori, A. M. Andrews, and G. Strasser, Polaritonic spectroscopy of intersubband transitions, *Phys. Rev. B* **86**, 125314 (2012).
- [45] K. Hennessy, A. Badolato, M. Winger, D. Gerace, M. Atatüre, S. Gulde, S. Fält, E. L. Hu, and A. Imamoglu, Quantum nature of a strongly coupled single quantum dot-cavity system, *Nature (London)* **445**, 896 (2007).
- [46] V. N. Pustovit and T. V. Shahbazyan, Cooperative emission of light by an ensemble of dipoles near a metal nanoparticle: The plasmonic dicke effect, *Phys. Rev. Lett.* **102**, 077401 (2009).
- [47] V. N. Pustovit and T. V. Shahbazyan, Plasmon-mediated super-radiance near metal nanostructures, *Phys. Rev. B* **82**, 075429 (2010).
- [48] T. Neuman and J. Aizpurua, Origin of the asymmetric light emission from molecular exciton-polaritons, *Optica* **5**, 1247 (2018).
- [49] G. Zengin, M. Wersäll, S. Nilsson, T. J. Antosiewicz, M. Käll, and T. Shegai, Realizing strong light-matter interactions between single-nanoparticle plasmons and molecular excitons at ambient conditions, *Phys. Rev. Lett.* **114**, 157401 (2015).
- [50] R. D. Artuso and G. W. Bryant, Optical response of strongly coupled quantum dot-metal nanoparticle systems: Double peaked Fano structure and bistability, *Nano Lett.* **8**, 2106 (2008).
- [51] N. Liu, L. Langguth, T. Weiss, J. Kästel, M. Fleischhauer, T. Pfau, and H. Giessen, Plasmonic analogue of electromagnetically induced transparency at the drude damping limit, *Nat. Mater.* **8**, 758 (2009).
- [52] G. Rempe, H. Walther, and N. Klein, Observation of quantum collapse and revival in a one-atom maser, *Phys. Rev. Lett.* **58**, 353 (1987).
- [53] D. S. Dovzhenko, S. V. Ryabchuk, Y. P. Rakovich, and I. R. Nabiev, Light-matter interaction in the strong coupling regime: Configurations, conditions, and applications, *Nanoscale* **10**, 3589 (2018).
- [54] F. Würthner, T. E. Kaiser, and C. R. Saha-Möller, J-aggregates: From serendipitous discovery to supramolecular engineering of functional dye materials, *Angew. Chem. Int. Ed.* **50**, 3376 (2011).
- [55] R. Hammaker, S. Francis, and R. Eischens, Infrared study of intermolecular interactions for carbon monoxide chemisorbed on platinum, *Spectrochim. Acta* **21**, 1295 (1965).
- [56] J. Zirkelbach, M. Mirzaei, I. Deperasińska, B. Kozankiewicz, B. Gurlek, A. Shkarin, T. Utikal, S. Götzinger, and V. Sandoghdar, High-resolution vibronic spectroscopy of a single molecule embedded in a crystal, *J. Chem. Phys.* **156**, 104301 (2022).
- [57] R. Chikkaraddy, B. de Nijs, F. Benz, S. J. Barrow, O. A. Scherman, E. Rosta, A. Demetriadou, P. Fox, O. Hess, and J. J. Baumberg, Single-molecule strong coupling at room temperature in plasmonic nanocavities, *Nature (London)* **535**, 127 (2016).
- [58] K. Santhosh, O. Bitton, L. Chuntonov, and G. Haran, Vacuum Rabi splitting in a plasmonic cavity at the single quantum emitter limit, *Nat. Commun.* **7**, 11823 (2016).
- [59] Y. Zhang, Q.-S. Meng, L. Zhang, Y. Luo, Y.-J. Yu, B. Yang, Y. Zhang, R. Esteban, J. Aizpurua, Y. Luo, J.-L. Yang, Z.-C. Dong, and J. G. Hou, Sub-nanometre control of the coherent interaction between a single molecule and a plasmonic nanocavity, *Nat. Commun.* **8**, 15225 (2017).
- [60] J. Le Gall, M. Olivier, and J.-J. Greffet, Experimental and theoretical study of reflection and coherent thermal emission by a SiC grating supporting a surface-phonon polariton, *Phys. Rev. B* **55**, 10105 (1997).